AD-A141 203 STUDY OF AVALANCHE DISCHARGE LASERS(U) CALIFORNIA UNIV 1/2
SAN DIEGO LA JOLLA INST FOR PURE AND APPLIED PHYSICAL
SCIENCES S C LIN 30 SEP 83 N00014-76-C-0116

UNCLASSIFIED F/G 20/5 NL

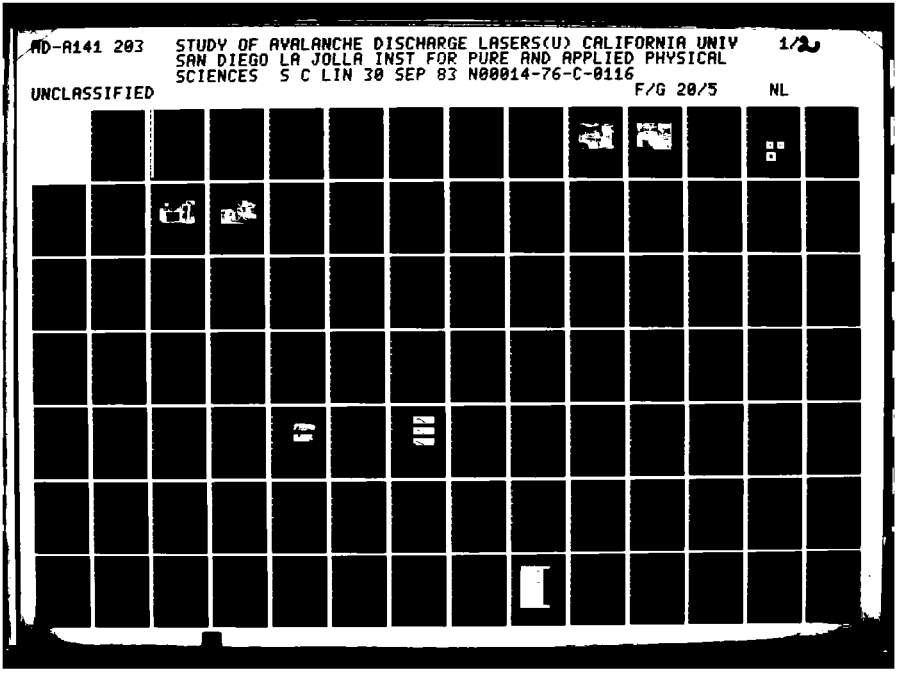

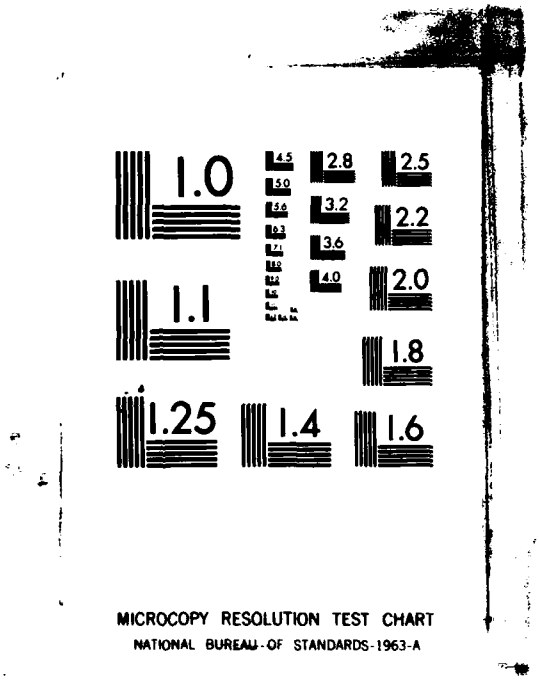

(12)

STUDY OF AVALANCHE DISCHARGE LASERS

Final Technical Report

Prepared by

Shao-Chi Lin

Institute for Pure and Applied Physical Sciences
University of California, San Diego
La Jolla, California 92093

for

Work supported by the Defense Advanced Research Projects Agency and monitored by the Office of Naval Research through Contract N00014-76-C-0116 for the period

July 1, 1975 through September 30, 1983

TABLE OF CONTENTS

		Page
	Abstract	1
I.	INTRODUCTION	2
	References	14
II.	TIME BEHAVIOR OF SECOND-POSITIVE EMISSIONS FROM A FAST-DISCHARGE $N_2 + SF_6$ LASER	17
III.	EFFECTS OF FIELD BROADENING AND PUMP LINE SELECTION ON MULTI-LEVEL ABSORPTION IN MOLECULAR SYSTEMS	18
IV.	OPTIMAL TIMING AND POWER ENHANCEMENT OBSERVED IN A DOUBLE-PULSE FAST-DISCHARGE-DRIVEN XeF LASER	20
V.	ELECTRON-BEAM-CONTROLLED DISCHARGE XeCl EXCIMER LASER	21
VI.	ELECTRON VELOCITY AND ENERGY DISTRIBUTIONS IN A HOMOGENEOUS AVALANCHE DISCHARGE - WITH APPLICATION TO RARE GAS HALIDE LASER EXCITATION	22
VII.	AN EXPERIMENTAL STUDY OF OPTICAL PHASE FLUCTUATIONS IN A RANDOM REFRACTIVE FIELD	24
VIII.	X-RAY PREIONIZATION FOR ELECTRIC DISCHARGE LASERS	26

TABLE OF CONTENTS (Continued)

Page

IX. NECESSARY CONDITIONS FOR THE HOMOGENEOUS FORMATION OF PULSED AVALANCHE DISCHARGES AT HIGH GAS PRESSURES 27

X. LONG PULSE BEHAVIOR OF THE AVALANCHE/SELF-SUSTAINED DISCHARGE PUMPED XeCl LASER 28

XI. CURRENT DENSITY AND PRESSURE DEPENDENCE OF XeCl EXCIMER FLUORESCENCE AND LASER EMISSIONS OBSERVED IN A VERY SMALL VOLUME DISCHARGE 29

XII. A THEORETICAL STUDY OF THE KINETIC PROCESSES IN A HIGH-POWER XENON CHLORIDE EXCIMER LASER OSCILLATOR DRIVEN BY A LONG TRANSMISSION LINE PULSE FORMING NETWORK 30

XIII. METHOD FOR DETERMINATION OF CO-SPECTRAL GAIN AND ABSORPTION COEFFICIENTS IN HIGH-POWER LASERS 33

References for Section XIII 72

XIV. REVERSAL OF SPECTRAL NARROWING OF XENON CHLORIDE $B\,^2\Sigma \rightarrow X\,^2\Sigma$ EMISSION OBSERVED AT HIGH GAS PRESSURES 75

References for Section XIV 104

STUDY OF AVALANCHE DISCHARGE LASERS

Shao-Chi Lin

University of California, San Diego

La Jolla, California 92093

Abstract

The basic research carried out at the University of California, San Diego, on the study of avalanche discharge lasers with partial, and at times intermittent, funding support from the Defense Advanced Research Projects Agency under Contract N00014-76-C-0116 over an eight-year period, 1975 - 1983, is summarized. This research has resulted in many important scientific discoveries and generated much basic data which are of great value in the engineering development of high-power, short-wavelength gas lasers. The most noteworthy of these is our discovery that X-ray is far superior to both ultraviolet light and electron beams as a preionization source for homogeneous initiation of very large volume, pulsed avalanche discharges at high gas pressures. Another important discovery is that such pulsed discharges can be stably sustained at high current densities over relatively long periods of time (~ hundreds of nsec) using suitable pulse forming networks. However, in the case of the rare gas halogen excimers, the laser pulse duration is often kinetics-limited.

I. INTRODUCTION

The effectiveness of high current density pulsed avalanche discharges in the excitation of high-power, short-wavelength, electronic-transition gas lasers was first demonstrated by Leonard in 1965.[1] Using molecular nitrogen at 20 torr initial pressure in a transverse discharge of 0.3 x 2.5 x 200 cm^3 dimensions (0.15 liter total volume), ~ 0.7 kA/cm^2 peak current density, and ~ 100 nsec duration, Leonard had observed peak laser output power of up to 200 kW and 20 nsec duration from the second-positive band of N_2 in the near ultraviolet ($\lambda \sim$ 337.1 nm). The maximum pressure that can be used for homogeneous formation of a short duration (~ 20 nsec) pulsed avalanche discharge of comparable dimensions in N_2 and in N_2/SF_6 gas mixtures has subsequently been extended to about 200 torr by the research group at UC San Diego in 1974 through the use of a synchronous uv preionization pulse in conjunction with a fast-rise-time, distributed Blumlein-type discharge circuit.[2, 3] The observed peak power output of the N_2 ultraviolet laser was accordingly increased to the 3 MW level at a single-pulse energy conversion efficiency, η_E [defined here as the laser output pulse energy/initial energy storage in the PFN (Pulse Forming Network)], of about 0.1%. In addition to these earlier nitrogen laser experiments, the use of such fast-rise-time pulsed avalanche discharge ("fast discharge") for the pumping of other high power, short-wavelength, electronic-transition gas lasers, including the more recently discovered rare gas halide and mercury halide excimer lasers, have also been reported by many investigators.[4 - 15] Due to the limited range of ultraviolet light as a preionization source in high

pressure gases, however, the homogeneous avalanche volume in these reported experiments was generally quite small (typically, some minor fraction of 1 liter).

It should be mentioned in passing that transverse discharges have been used for the pumping of long-wavelength ($\lambda \sim 10.6\ \mu m$) CO_2 laser at high gas pressures since 1970.[16,17] However, the optimum field strength for efficient pumping of this vibrational/rotational-transition laser is significantly below the avalanche threshold.[18] Accordingly, the most suitable discharge for efficient, high-power pumping of the CO_2 laser is of the artificially-sustained type, such as by a high-voltage, electron-beam source introduced into the high-pressure gas through a thin foil-window for maintaining a steady-state number density of free electrons .[19] For pumping of some rare gas halogen excimer lasers, especially XeCl , the electron-beam-sustained discharge experiments at UC San Diego[20] indicated that at a fixed e-beam current density, the XeCl laser power output and generation efficiency tended to increase rapidly and monotonically with the field strength to gas density ratio E/n , starting from E/n = 0 and continuing up to the avalanche threshold. This suggested that for the excitation of most high-power, short-wavelength, electronic-transition lasers, the optimum E/n and current density are above the avalanche threshold and beyond what can be conveniently provided by an externally-sustained electrical discharge.

In 1977, the use of X-ray as a preionization source for homogeneous initiation of large volume, high pressure, pulsed avalanche discharges was proposed by Principal Investigator (author of this Final Technical Report)

at UC San Diego.[21] (Actually, a proposal to explore this same idea was submitted by the Principal Investigator to the Defense Advanced Research Projects Agency as early as 1974, but no serious work was started at that time due to a lack of funding support.) In 1978, with the basic research support from DARPA under Contract N00014-76-C-0116 and a small ($20K) but crucial supplemental funding from the Office of Naval Research under Contract N00014-77-C-0692, the Principal Investigator and his graduate student Jeffrey I. Levatter at UC San Diego had achieved an important breakthrough in demonstrating not only that the X-ray preionization idea really worked, but also that the laser performance resulting from the use of this preionization method in conjunction with a low-impedance, transmission-line-type pulse forming network for sustaining the discharge current and a short-rise-time, rail-gap-type switch for sudden application of the super-avalanche field-strength E, had far exceeded what could be expected from the initial experiments.[22]

The X-ray preionized discharge system constructed at UC San Diego and used in the first demonstration experiments just mentioned[22] is illustrated in Fig. 1. The gas handling system, also constructed with primary funding support from Contract N00014-76-C-0116 for the study of high-power lasers involving halogen and other corrosive gases, is shown in Fig. 2. Using the discharge system illustrated in Fig. 1 with a 0.5Ω water-dielectric transmission line and associated electrical circuits shown in the schematic diagrams, Figs. 3(a) and (b), it was found that spatially homogeneous, pulsed avalanche discharges of up to 2.5 liter volume can readily be generated

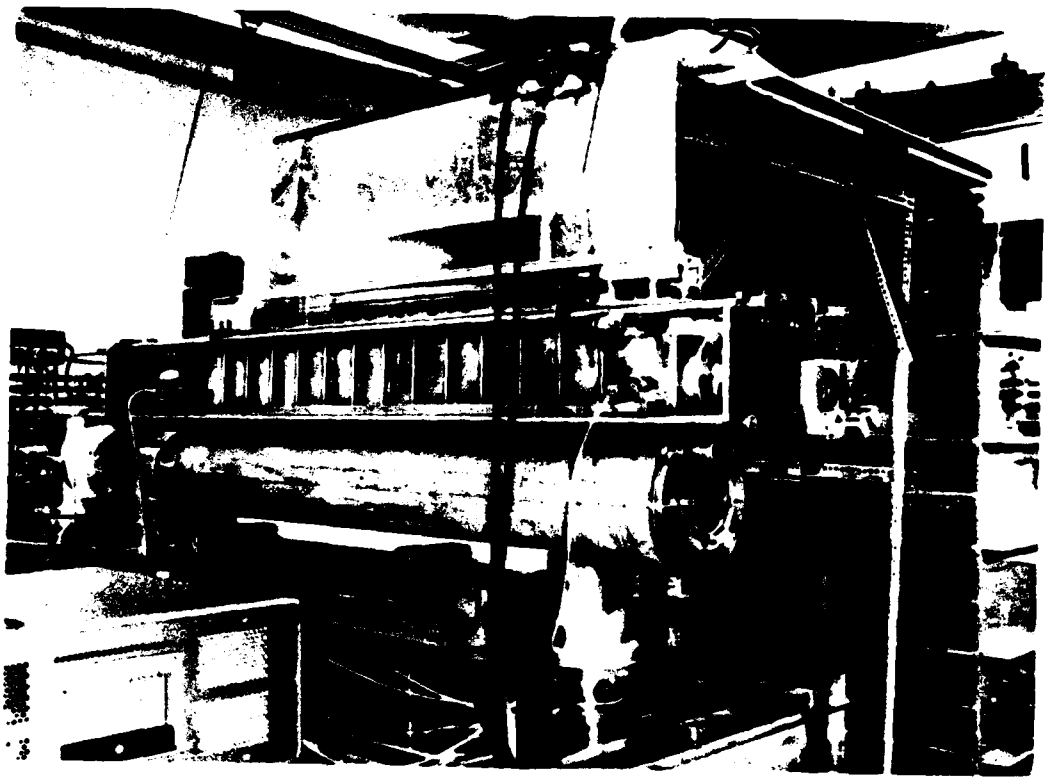

Fig. 1 Photograph of the multi-liter-volume, x-ray preionized, pulsed avalanche/self-sustained discharge apparatus at UC San Diego.

Fig. 2 Gas handling system and control panel for the x-ray preionized, pulsed avalanche/self-sustained discharge apparatus at UC San Diego.

in several rare gas-halogen mixtures at 1 atm initial pressure. The discharge was also found to be temporally stable over the 100 nsec pulse duration corresponding to the electrical length (2-way wave propagation time) of the transmission line. The ultraviolet XeCl, XeF, and KrF laser output beams were of uniform intensity over a cross-sectional area comparable to that of the homogeneous discharge (Fig. 4). The laser output power observed during the stably-sustained phase of the discharge was approximately 20 MW. The corresponding single-pulse energy conversion efficiency, η_E, was about 1.4%. A smaller volume ($\sim$ 0.18 liter) X-ray preionized discharge experiment was also reported by Sumida, Obara, and Fujioka in 1978,[23] with KrF laser output pulse energy of up to about 80 mJ over a pulse width of $\sim$ 30 nsec (i.e., $\sim$ 3 MW peak power) at an energy conversion efficiency of about 1%.

The experimental pressure range for X-ray preionized pulsed avalanche discharges in rare gas-halogen mixtures was extended to about 5 atm by a research group at the Shanghai Institute of Optics and Fine Mechanics, Shanghai, China, in 1980.[24] Using a highly diluted Ne/Xe/HCl mixture in a 0.19 liter volume discharge of $\sim$ 70 nsec duration, the XeCl laser output at 308 nm was found to increase linearly with the gas pressure at a fixed transmission line charging voltage (or, equivalently, at a fixed current density, since the plasma resistance was considerably lower than the line impedance). At a fixed gas pressure, the laser output was found to increase linearly with the charging voltage or current density. The observed specific power output of the XeCl laser per liter of discharge volume was about

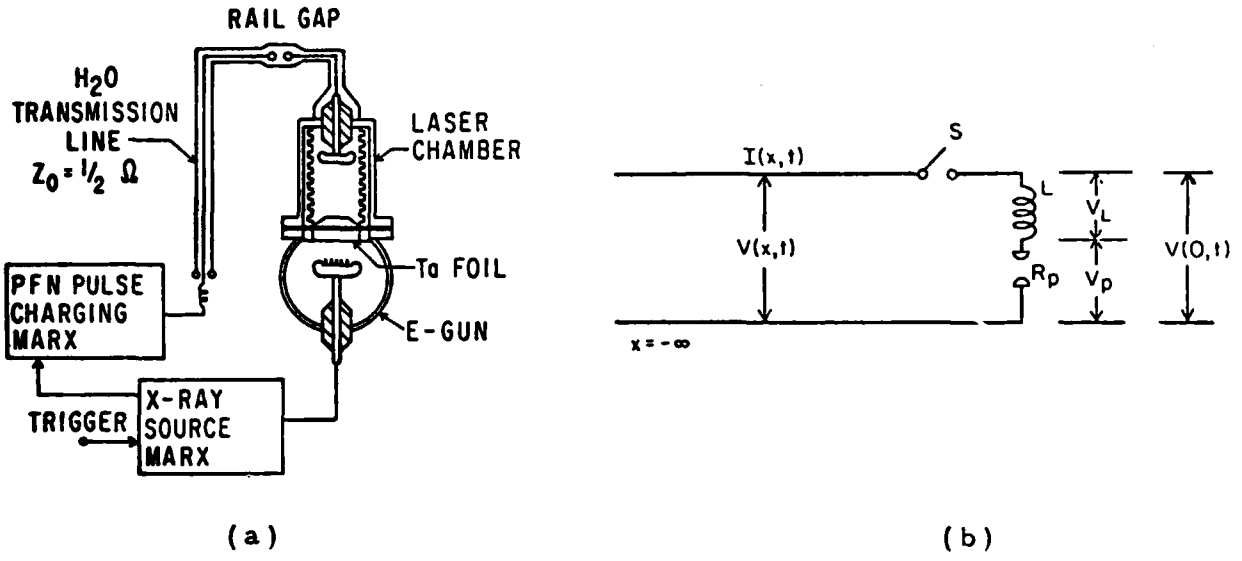

Fig. 3 (a) Schematic drawing, and (b) equivalent circuit of the X-ray preionized, pulsed avalanche discharge apparatus used by Lin and Levatter (Ref. 22) for the generation of homogeneous-volume, high-pressure discharges at UC San Diego.

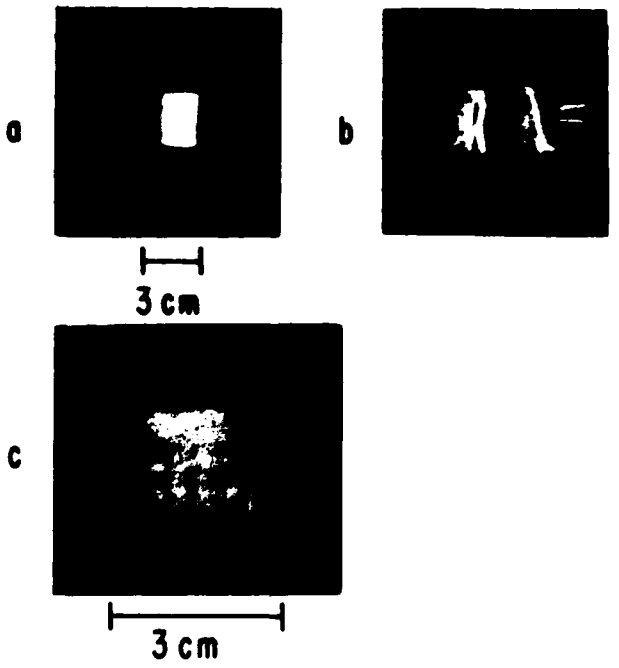

Fig. 4 Top row: Pol id photographs showing (a) homogeneou discharge with X-ray p nization and (b) inhomogeneous discha e in the absence of X-r reionization. Bottom picture: uv burn pattern on Polaroid filn get from the output beam of a single-pulse, X-ray preionized ra gas halide excimer laser discharge. (From Ref. 22.)

100 MW at the highest gas pressure ($\sim$ 5 atm) and current density ($\sim$ 1 kA/cm^2) tested in one of the gas mixtures. These results are of considerable engineering significance since, according to the analysis of Levatter and Lin,[25] one should be able to generate homogeneous pulsed avalanche discharges of very large volume at a very low cost of preionization energy (e.g., $n_{eo} \sim 10^6$ electrons/cm^3, or approximately 0.1 mJ/liter, assuming an X-ray generation/utilization efficiency[22] of 0.005%, and an energy cost of $\sim$ 30 eV to produce an electron-ion pair). Thus, if the 100 MW/liter specific power output observed in Ref. 24 can be maintained over pulse durations of the order of 1 μsec as has been observed in some electron-beam-pumped XeF laser experiments,[26] generation of 1 to 10 kJ uv laser pulses of interest in inertial confinement fusion research (assuming sufficiently high pulse-compression efficiency)[27, 28] may require a very modest homogeneous discharge volume of only 10 to 100 liters. In comparison with the alternative e-beam method for large volume pumping of the rare gas halogen excimer lasers,[11] the X-ray preionized discharge method appears to offer the advantage of being compatible with high pulse-repetition-rate operations commonly required in most engineering applications due to the absence of any fragile foil windows in the latter method of excitation.[22]

The long pulse behavior of the X-ray preionized, pulsed avalanche/self-sustained discharge-pumped XeCl laser has been studied by Levatter, Robertson, and Lin at UCSD in 1981,[29] using the experimental arrangement described in Ref. 22 (Fig. 3) but with the electrical length of the water-dielectric transmission line extended to 200 nsec. The discharge was

found to be homogeneous and stable over the whole 200 nsec duration for all the gas samples tested (He/Xe/HCl and Ne/Xe/HCl mixtures of various mol ratios at gas pressures between 1 and 3 atm). However, the XeCl laser output power and waveform were found to be sensitive to the mixture composition and gas pressure. In particular, at the higher gas pressures, the laser power output was found to fall off rapidly before the stably self-sustained discharge was terminated in some of the gas mixtures. Such premature termination of the laser pulse was not caused by a sudden depletion of the HCl mol fraction during the discharge. Instead, it was quite possibly a quenching phenomenon associated with some as yet unidentified reaction product or products generated by the gain-switching process or by some higher-order chemical reactions in the discharge plasma. This conclusion, which was drawn from the computational results of an elaborate computer code developed by the Principal Investigator and his graduate students at UC San Diego[30, 31] for tracking the energy transfer processes and plasma chemistry during the transient discharge, is quite different from the suggestion made by Hogan et al[32] that a similar premature termination of both the XeCl spontaneous emission and laser pulses observed in their small volume ($\sim$ 0.017 liter), resistively-ballasted, pin-electrode discharge can be explained in terms of HCl depletion in the active volume even though the specific electric power input rate in their experiment (270 kW/cm^3) was only about one-half the power input rate in the experiments reported in Ref. 29.

The behavior of XeCl excimer fluorescence and laser emissions at very high gas pressures ($2 < p < 15$ atm) and current densities ($0.6 < j < 2$

kA/cm^2) was studied by Lou, He, and Lin in 1982[33] using a very small volume, high-pressure discharge system recently constructed at UC San Diego with partial funding support from the Office of Naval Research under Contract N00014-79-C-0955 (Fig. 5). Premature termination of both the XeCl fluorescence and laser pulses were again observed and found to be more severe at the higher gas pressures and current densities. A good understanding of this premature pulse-termination phenomenon is obviously important for the future development of this high power excimer laser not only from the point of view of increasing the pulse energy output per unit volume, but also from the point of view of increasing the laser generation efficiency. As noted in Ref. 29, a single-pulse energy conversion efficiency of about 4% can already be obtained from the XeCl $B \rightarrow X$ ultraviolet laser using the sampled gas mixture Ne : Xe : HCl = 989 : 10 : 1 if the discharge pulse duration is matched to the laser pulse duration and if the transmission line impedance is properly matched to the plasma resistance. Further research in this area may well lead to new choices of gas mixtures and/or discharge parameters which would allow operations of this very promising class of high-power, short-wavelength lasers at even higher energy conversion efficiencies. Unfortunately, this work could not have been completed prior to the termination of the present research contract.

In addition to the pulse-termination phenomenon just mentioned, there were two other interesting research topics related to the XeCl laser in progress but also could not have been completed prior to the termination of the present contract. One is the determination of the co-spectral gain and

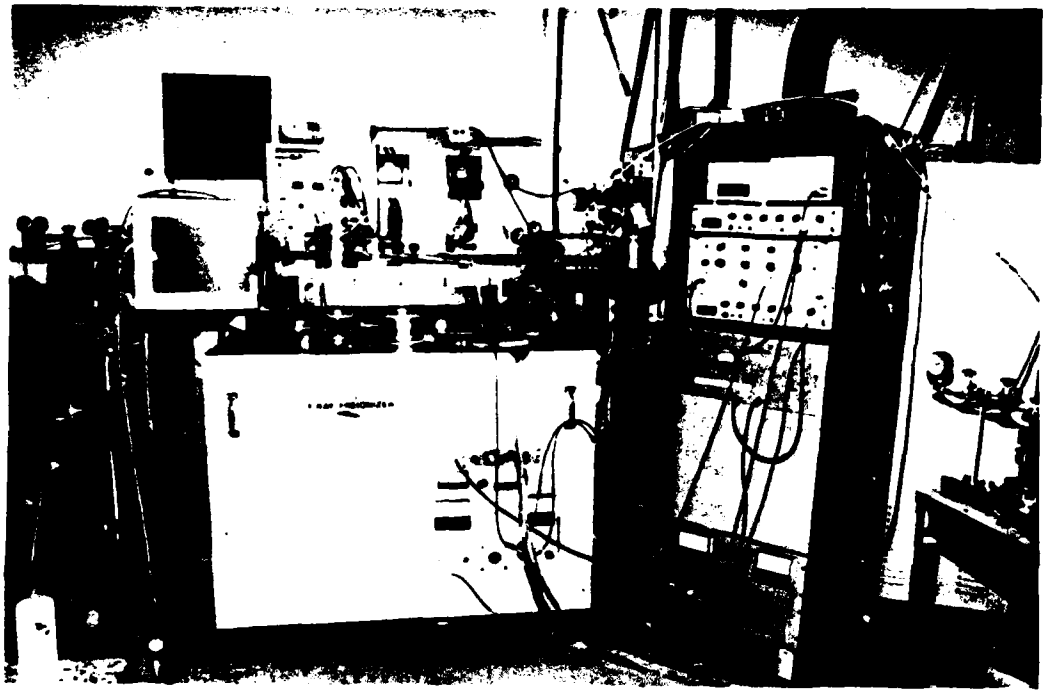

Fig. 5(a) Photograph of the recently constructed, small-volume, high-pressure discharge system at UC San Diego. The low energy x-ray preionization source ($\sim$ 1 J per pulse input energy to a $\sim$ 50 kV e-beam for the generation of forward-scattered x-rays from a 7.6-μm-thick tantalum foil target) is switched by a hydrogen thyratron and can be operated in a repetitively pulsed mode. Control panel is shown on the right. Gas samples are drawn from the mixing system shown in Fig. 2.

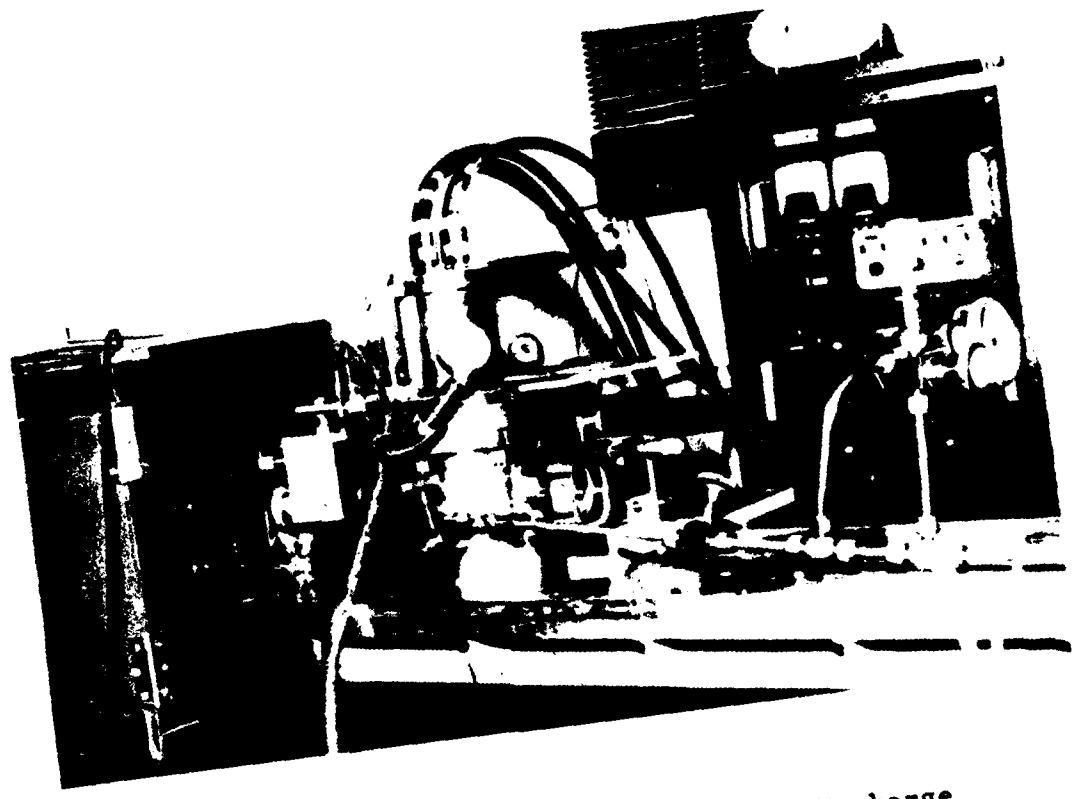

Fig. 5(b) Close-up view of the small cylindrical discharge chamber on top of the low energy x-ray preionization source with associated optical components used for observation of XeCl excimer fluorescence and laser emissions at very high gas pressures and current densities.

absorption coefficients in the discharge-excited plasma. The other is the variation of FWHM width of the XeCl B → X spontaneous emission spectrum with gas pressure and mixture composition. Both topics are very much relevant to the problem of mode-buildup-time and optical-power-extraction efficiency under various excitation conditions.

In the sections that follow, all the essential results from the research work performed at UC San Diego, whether supported in whole or in part under Contract N00014-76-C-0116, are summarized. To avoid unnecessary duplication, research results which have already been reported in the form of published papers in archive journals or in the form of doctoral dissertations are summarized by brief abstracts under the respective titles together with the names of authors, date and place of publication. Research results not yet published, on the other hand, are presented in the last two sections as full manuscripts being prepared for journal publication.

References

1. D. A. Leonard, Appl. Phys. Lett. 7, 4 (1965).
2. J. I. Levatter and S. C. Lin, Appl. Phys. Lett. 25, 703 (1974).
3. R. P. Akins and S. C. Lin, Appl. Phys. Lett. 28, 221 (1976).
4. C. P. Wang, H. Mirels, D. G. Sutton, and S. N. Suchard, Appl. Phys. Lett. 28, 326 (1976).
5. R. Burnham, F. Y. Powell, and N. Djeu, Appl. Phys. Lett. 29, 30 (1976).

6. J. I. Levatter and R. S. Bradford, Jr., Appl. Phys. Lett. 33, 742 (1978).

7. R. C. Sze and P. B. Scott, Rev. Sci. Instrum. 49, 772 (1978).

8. R. P. Akins, G. Innis, and S. C. Lin, J. Appl. Phys. 49, 2262 (1978).

9. E. J. Schimitschek and J. E. Celto, Optics Lett. 2, 64 (1978).

10. C. A. Brau, "Rare Gas Halogen Excimers," Chapter 4 in Vol. 30 of Topics in Applied Physics, Excimer Lasers (Editor: C. K. Rhodes), Springer-Verlag, Berlin, Heidelberg, New York (1979).

11. C. H. Fisher, R. E. Center, G. J. Mullaney, and J. P. McDaniel, Appl. Phys. Lett. 35, 26 (1979).

12. R. Burnham, Appl. Phys. Lett. 35, 48 (1979).

13. R. C. Sze, IEEE J. Quantum Electron. QE-15, 1338 (1979).

14. W. J. Sarjeant, A. J. Alcock, and K. E. Leopold, IEEE J. Quantum Electron. QE-14, 177 (1978).

15. S. Watanabe, A. J. Alcock, K. E. Leopold, and R. S. Taylor, Appl. Phys. Lett. 38, 3 (1981).

16. A. J. Beaulieu, Appl. Phys. Lett. 16, 504 (1970).

17. A. J. DeMaria, Proc. IEEE 61, 731 (1973).

18. W. L. Nighan and J. H. Bennett, Appl. Phys. Lett. 8, 240 (1969).

19. R. M. Patrick, D. H. Douglas-Hamilton, and S. A. Mani, J. Appl. Phys. 45, 4406 (1974).

20. J. I. Levatter, J. H. Morris, and S. C. Lin, Appl. Phys. Lett. 32, 630 (1978).

21. S. C. Lin, "X-ray Preionization for Excimer Laser Generation," University of California, San Diego, Proposal No. UCSD-9862, submitted to the Office of Naval Research April 1, 1977 and funded September 1, 1977.

22. S. C. Lin and J. I. Levatter, "X-ray Preionization for Electric Discharge Lasers," Final Technical Report for work supported by the Office of Naval Research under Contract N00014-77-C-0692, June 1978; also Appl. Phys. Lett. 34, 505 (1979).

23. S. Sumida, M. Obara, T. Fujioka, Appl. Phys. Lett. 33, 913 (1978).

24. S. C. Lin, Z. X. Bao, G. Y. Gong, Y. S. Huo, J. P. Shu, S. Q. Tang, Y. R. Wei, and C. E. Zheng, Appl. Phys. Lett. 38, 328 (1981).

25. J. I. Levatter and S. C. Lin, J. Appl. Phys. 51, 210 (1980).

26. L. F. Champagne, J. G. Eden, N. W. Harris, N. Djeu, and S. K. Searles, Appl. Phys. Lett. 30, 160 (1977).

27. K. A. Brueckner and S. Jorna, Rev. Mod. Phys. 46, 325 (1974).

28. J. Goldhar, W. R. Rapoport, and J. R. Murray, IEEE J. Quantum Electron. QE-16, 235 (1980).

29. J. I. Levatter, K. L. Robertson, and S. C. Lin, Appl. Phys. Lett. 39, 297 (1981).

30. H. H. Luo, Ph. D. Dissertation, University of California, San Diego (1978).

31. Y. S. Wang, Ph. D. Dissertation, UC San Diego (1982).

32. D. C. Hogan, R. Bruzzese, A. J. Kearsley, and C. E. Webb, J. Phys. D: Appl. Phys. 14, L157 (1981).

33. Q. H. Lou, Q. S. He, and S. C. Lin, Appl. Phys. Lett. 41, 514 (1982).

II. TIME BEHAVIOR OF SECOND-POSITIVE EMISSIONS FROM A FAST-DISCHARGE $N_2 + SF_6$ LASER* (R. P. Akins and S. C. Lin, paper published in Applied Physics Letters, Vol. 28, No. 4, 15 February 1976, pp. 221 - 223)

Summary

The time behavior of spectrally resolved N_2 second-positive emissions recently observed in our fast-discharge $N_2 + SF_6$ laser reveals some surprising features that cannot be explained on the basis of SF_6 - catalyzed vibrational relaxation or collisional quenching of the lower-laser-level $B\,^3\Pi_u$. Instead, they suggest the existence of an extremely fast excitation process for the upper-laser-level $C\,^3\Pi_u$ involving SF_6 as an intermediary, although the kinetic path for such a process remains unclear.

*Work supported by the Defense Advanced Research Projects Agency and monitored by the Office of Naval Research under Contract N00014-76-C-0116.

III. EFFECTS OF FIELD BROADENING AND PUMP LINE SELECTION ON MULTI-LEVEL ABSORPTION IN MOLECULAR SYSTEMS**

(S. C. Lin and J. H. Morris, paper published in Journal of Quantitative Spectroscopy and Radiative Transfer, Vol. 17, No. 5, May 1977, pp. 577 - 593)

Summary

The problem of multi-level absorption of i. r. laser radiation in polyatomic gases is examined using the density matrix formalism. The general condition under consideration is that field broadening effects are significant, but the detailed and discrete features of the absorption spectra remain very important. Collisional effects are taken into account through macroscopic relaxation terms, but the cumulative effects of collisional relaxation are assumed to cause only minor perturbations to the overall vibrational-rotational populations over the optical pumping time scale of interest. Various approximate formulae are then derived for locating the optimum frequency for optical pumping of three consecutive anharmonic vibrational levels within a given normal mode and for predicting the intensity- and frequency-dependence of the resultant uppermost level population density during a quasi-steady state balance among the absorption, stimulated emission, dephasing collision and rotational

** Work supported, in part, by the Defense Advanced Research Projects Agency and monitored by the Office of Naval Research under Contract N00014-76-C-0116.

relaxation rates. Numerical examples are illustrated for pumping of the three lowest vibrational levels within the non-degenerate asymmetric stretching mode of the linear triatomic molecule CO_2 for which the absorption spectra are relatively simple and well known. Some possible applications of these results to the problem of i. r. laser frequency conversion and to the interpretation of wavelength-selective i. r. photodissociation recently observed in many symmetric top molecules, such as BCl_3 , SiF_4 and SF_6 for which the absorption spectra are much more complex and the spectroscopic constants much less certain, are also discussed.

IV. OPTIMAL TIMING AND POWER ENHANCEMENT OBSERVED IN A DOUBLE-PULSE FAST-DISCHARGE-DRIVEN XeF LASER[†]

(R. P. Akins, G. Innis, and S. C. Lin, paper published in the Journal of Applied Physics, Vol. 49, No. 4, April 1978, pp. 2262-2264)

Summary

A surprisingly long delay time (of the order of 10 μsec) is found necessary for maximum enhancement of the output power and energy from the main pulse of a 0.1-liter-volume Blumlein-driven XeF excimer laser when another fast-discharge pulse of about 0.1-μsec duration and 10% of the main discharge energy is used to preionize or otherwise "precondition" the gas mixture. At such optimal timing, a factor-of-5 enhancement of the UV laser output ($3510 < \lambda < 3537$ Å) has been observed in a $He:Xe:NF_3$ mixture at an overall generation efficiency of 1.3%.

[†]Work supported jointly by the U.S. Energy Research and Development Administration through the Lawrence Livermore Laboratory Purchase Order No. 3216503 for Contract W-7405-ENG 48 and the Defense Advanced Research Projects Agency under Contract N00014-76-C-0116 monitored by the Office of Naval Research.

V. ELECTRON-BEAM-CONTROLLED DISCHARGE XeCl EXCIMER LASER[‡] (J. I. Levatter, J. H. Morris, and S. C. Lin, paper published in the Applied Physics Letter, Vol. 32, No. 10, 15 May 1978, pp. 630 - 632)

Summary

A large-volume (6 - liter) electron-beam-controlled discharge of about 1 μsec duration in a Xe/Ar mixture with HCl as the chlorine donor has been utilized to achieve efficient XeCl laser generation at 3080 Å. At a fixed gas pressure and e-beam current, the laser output is found to increase rapidly with the initial sustainer field strength up to the spontaneous breakdown limit. Near such a limit, a factor-of- 25 enhancement of the XeCl laser output energy over that due to e-beam pumping alone has been observed at 1 atm total pressure. The specific output pulse energy density and laser efficiency based on total energy deposition, of 0.5 J/liter atm and 0.7%, respectively, are beginning to approach the best values reported in the literature for the XeF and KrF lasers.

[‡] Work supported by the Defense Advanced Research Projects Agency under Contract N00014-76-C-0116 monitored by the Office of Naval Research.

VI. ELECTRON VELOCITY AND ENERGY DISTRIBUTIONS IN A HOMOGENEOUS AVALANCHE DISCHARGE - WITH APPLICATION TO RARE GAS HALIDE LASER EXCITATION*

(H. H. Luo, Ph. D. Dissertation, University of California, San Diego, 1978; University Microfilms Dissertation Copies Order Number 79-04141, P. O. Box 1764, Ann Arbor, Michigan 48106)

Summary

The problem of determining the electron velocity and energy distribution functions during transient avalanche discharges in gas mixtures with many elastic and inelastic collision processes is examined. The single-electron distribution functions are obtained by numerical solution of the Maxwell-Boltzmann equation under the following assumptions: (1) The gas is homogeneous in space and the electric field is constant in direction and also spatially uniform. (2) The fractional changes of the electric field and electron number density (caused by the ionization, recombination, and attachment processes) within the average time between two successive collisions of an electron are very small. That is, $|\, d\ell n E/dt \,| \cdot \tau_{coll} \ll 1$, $|\, d\ell n n_e/dt \,| \cdot \tau_{coll} \ll 1$, so that a quasi-steady-state distribution of elec-

*Work supported, in part, by the Defense Advanced Research Projects Agency and monitored by the Office of Naval Research under Contract N00014-76-C-0116.

tron energy exists at all times. (Here, E denotes the electric field strength, n_e is the number density of free electrons, and τ_{coll} is the mean collision time of the free electrons in the gas mixture.) The validity of the second assumption has been verified through numerical solution of some typical examples of fast discharges with current rise times and pulse durations of the order of 10^{-8} sec (10 nsec). Sample solutions of the electron energy distribution functions in discharges in pure He and in $He/Xe/F_2$ mixtures are obtained. From these distribution functions, the mean electron energy, the mean electron drift velocity, the rate coefficient for each process, and the electron avalanche (or decay) rate are also obtained. The electron-electron and electron-ion Coulomb collisions, important at high degrees of ionization in any gas mixture, are included in these calculations.

The numerical solutions of the Boltzmann equation are applied to the study of the excitation processes in fast-discharge-driven XeF excimer lasers. From the electron energy distribution function, all the reaction rate coefficients in processes involving the free electrons can be obtained as functions of E/n (ratio of the electric field strength to the total molecular number density), and the species mol fractions in the excited plasma. The results are compared with experiments and with the results obtained by the moments method.

VII. AN EXPERIMENTAL STUDY OF OPTICAL PHASE FLUCTUATIONS IN A RANDOM REFRACTIVE FIELD**

(R. L. Sandstrom, Ph. D. Dissertation, University of California, San Diego, 1979; University Microfilms Dissertation Copies Order Number 79-21493, P. O. Box 1764, Ann Arbor, Michigan 48106)

Summary

A heated grid subsonic turbulence tunnel of 52×52 cm^2 cross section is used to study the phase perturbations induced in a laser beam by the random refractive field. The phase measurements are carried out by a dual-beam laser heterodyne interferometer specially built for the experiment. The interferometer is capable of probing the refractive field along two parallel ray paths simultaneously, yielding single- and two-path statistics over a mutual separation distance which is variable from 1 mm to about 8 cm.

Measurements of the temperature field by fast platinum resistance probes show temperature fluctuations of up to 2 °C RMS at the highest grid heating rates (225 kW). Temperature structure functions indicate that the turbulence field is isotropic at least out to 7 cm length scale, and yield values of the refractive index structure constant C_n^2 varying from 4.9×10^{-12} to 3.6×10^{-11} m$^{-2/3}$, which is roughly two orders of magnitude greater than the highest values seen in the natural atmosphere. The temperature power

** Work supported by the Defense Advanced Research Projects Agency under Contract N00014-76-C-0116 monitored by the Office of Naval Research.

spectrum is found to exhibit a power-law region of the form $k^{-1.4}$ for nearly two decades in wavenumber, deviating somewhat from the $k^{-5/3}$ Obukhov-Corrsin spectrum expected for the inertial subrange.

Theoretical integral equations relating the single-point temperature fluctuation spectrum of arbitrary shape to several statistical functions of the phase fluctuation over a finite optical propagation length are developed and presented. Phase statistics measured include the RMS fluctuation amplitude, structure functions, absolute phase power spectrum, relative phase power spectrum for both longitudinal and transverse beam separations relative to the mean fluid flow, longitudinal space-time autocorrelation, phase, and coherence functions. The absolute phase power spectrum is found to adhere well to a power-law of the form $k^{-2.35}$ for nearly two decades in k.

Comparisons are made between experimentally measured phase fluctuation statistics and theoretical predictions by the integral relations using single-point temperature spectra measured concurrently with the optical phase data. The agreement in shape is excellent in all the statistical functions, but discrepancies in absolute magnitude attributed to calibration errors for one series of data are noted.

Taylor's frozen-flow assumption is investigated by using the wake-free probing capabilities of the interferometer. Studies of the coherence function indicate some non-frozen behavior. The phase function conforms surprisingly well to frozen-flow predictions, and no evidence is seen which might indicate a difference in phase speed between the various spectral components.

VIII. X-RAY PREIONIZATION FOR ELECTRIC DISCHARGE LASERS[†]

(S. C. Lin and J. I. Levatter, paper published in Applied Physics Letters, Vol. 34, No. 8, 15 April 1979, pp. 505 - 508)

Summary

Using x-rays of 60 - 200 keV photon energy ($\lambda \sim 0.06 - 0.2$ Å) as an ionizing radiation source in a transmission-line-driven low-inductance discharge chamber, we have succeeded in generating spatially homogeneous pulsed avalanche discharges of several liter volume at greater than 1 atm pressure for up to 100-nsec duration. In concurrent laser generation experiments with relatively lossy windows, we have observed high-optical-quality pulsed uv laser output of up to 2 J/liter from such discharges in rare-gas/halogen mixtures, and ir laser output of up to 12.5 J/liter from a $He/N_2/CO_2$ mixture.

[†]Work supported jointly by the Office of Naval Research under Contract N00014-77-C-0692 and by the Defense Advanced Research Projects Agency under Contract N00014-76-C-0116.

IX. NECESSARY CONDITIONS FOR THE HOMOGENEOUS FORMATION OF PULSED AVALANCHE DISCHARGES AT HIGH GAS PRESSURES[††]

(J. I. Levatter and S. C. Lin, paper published in the Journal of Applied Physics, Vol. 51, No. 1, January 1980, pp. 210 - 222)

Summary

The preionization level and other initial conditions necessary for the formation of spatially homogeneous pulsed avalanche discharges at high gas pressures are examined. Assuming properly shaped electrodes with no strong edge effects, the minimum preionization level required for homogeneous discharge initiation is found to depend on the voltage rise time across the electrodes as well as on the total pressure and various electrochemical properties of the gas mixture which govern the net rate of change of the first Townsend coefficient with respect to the local electric field strength. Our predictive results are found to be consistent with experimental observations.

[††]Work supported by the Defense Advanced Research Projects Agency under Contract N00014-76-C-0116 monitored by the Office of Naval Research.

X. LONG PULSE BEHAVIOR OF THE AVALANCHE/SELF-SUSTAINED DISCHARGE PUMPED XeCl LASER[‡]

(J. I. Levatter, K. L. Robertson, and S. C. Lin, paper published in Applied Physics Letters, Vol. 39, No. 4, 15 August 1981, pp. 297 - 299)

Summary

Homogeneous and stable avalanche/self-sustained discharges of 200-nsec duration have been obtained in typical XeCl laser gas mixtures at relatively high gas pressures (1 - 4 atm) and high energy loadings (100 - 400 J/liter-atm). The laser output waveform, however, is found to be surprisingly sensitive to changes in gas pressure and composition. Under certain conditions, the laser power remains nearly constant for 200 nsec, so that the total output energy scales roughly with the discharge duration. The highest XeCl laser pulse energy extracted from a 1-liter volume in this series of experiments is 3.2 J at ~ 4% intrinsic efficiency.

[‡] Work supported by the Defense Advanced Research Projects Agency under Contract N00014-76-C-0116 monitored by the Office of Naval Research.

XI. CURRENT DENSITY AND PRESSURE DEPENDENCE OF XeCl EXCIMER FLUORESCENCE AND LASER EMISSIONS OBSERVED IN A VERY SMALL VOLUME DISCHARGE* (Q. H. Lou, Q. S. He, and S. C. Lin, paper published in Applied Physics Letters, Vol. 41, No. 6, 15 September 1982, pp. 514 - 516)

Summary

Some observational results on the XeCl excimer $B \rightarrow X$ fluorescence and laser emissions from dilute Ne/Xe/HCl mixtures in a very small volume ($\sim 1\ cm^3$) pulsed avalanche discharge of ~ 200 nsec duration at high current densities ($0.6 < j < 1.8\ kA/cm^2$) and at high gas pressures ($2 < p < 11$ atm) are presented. With increasing j , p , and Ne dilution, the fluorescence pulse duration becomes more and more restricted but the laser peak power continues to show an upward trend until $p \approx 8$ atm. In spite of the short pulse and low extraction efficiency, laser peak power of up to ~ 10 kW has been observed from the $\sim 1\ cm^3$ volume discharge.

*Work supported, in part, by the Defense Advanced Research Projects Agency and monitored by the Office of Naval Research under Contract N00014-76-C-0116.

XII. A THEORETICAL STUDY OF THE KINETIC PROCESSES IN A HIGH-POWER XENON CHLORIDE EXCIMER LASER OSCILLATOR DRIVEN BY A LONG TRANSMISSION LINE PULSE FORMING NETWORK** (Y. S. Wang, Ph. D. Dissertation, University of California, San Diego, 1982; University Microfilms Dissertation Copies Order Number 82-24532, P. O. Box 1764, Ann Arbor, Michigan 48106)

Summary

A theoretical model of the discharge pumped XeCl laser driven by a long transmission line (two-way transit time, ~ 200 nsec) is presented. The mathematical formulation consisting of the rate equations, the temperature equation, the circuit equation, and the Boltzmann equation governing the velocity and energy distributions of the free electrons is developed under the assumptions that the applied electric field strength is spatially uniform and the number densities of all important chemical species are spatially homogeneous in the discharge volume. These coupled non-linear differential equations are solved numerically by using the GBS extrapolation method simultaneously with the time evolution of the electron mole fraction during the transient discharge. The time-dependent electron velocity and energy distribution functions are obtained from the numerical solutions of the Boltz-

**Work supported, in part, by the Defense Advanced Research Projects Agency under Contract N00014-76-C-0116 and by the Office of Naval Research under Contract N00014-80-C-0335.

mann equation, with all elastic (including electron-electron), inelastic, attachment, recombination, and ionization collisions included, by a self-consistent iteration technique.

The kinetic reactions involved in the XeCl laser using Ne/Xe/HCl and He/Xe/HCl mixtures are comprehensively examined. The results of this study reveal that the new processes

$$e + XeCl^* \longrightarrow Xe^* + Cl^- ,$$

$$e + XeCl \longrightarrow Xe + Cl^- \quad \text{or} \quad Xe + Cl + e ,$$

are important and have to be included in the model. In addition, the rate coefficients for the processes

$$e + HCl(v=1) \longrightarrow H + Cl^- ,$$

$$XeCl + Ne, He \longrightarrow Xe + Cl + Ne, He ,$$

$$h\nu + XeCl^* \longrightarrow XeCl^{**} ,$$

should be revised from the earlier published values. (Here, $XeCl^*$ denotes the XeCl $B\,^2\Sigma$ and $C\,^2\Pi$ excimer states, while $XeCl^{**}$ represents some unidentified, higher-lying excited states of the XeCl excimer which are optically-connected to $XeCl^*$.) The recommended revisions are discussed in detail in Chapter Five of this thesis.

A working kinetics model for quantitative interpretation of all the recent discharge-pumped high power XeCl excimer laser experiments is finally developed. According to this model, the rate limiting steps

which govern the discharge characteristics and the laser performance at the current density ($j \approx 300\ A/cm^2$) and gas pressures ($p = 1$ to 5 atm) used in these epxeriments are all two-body collisions in which the free electrons play the most important role in many aspects. Unlike common expectation, the number density of the laser upper state at a fixed discharge current density is found to be insensitive to the total gas pressure. Instead, the experimentally observed higher laser output power at the higher gas pressures is mainly due to the faster removal rate of the laser lower state population.

The close agreement between the calculated and measured waveforms of the discharge voltage, the side-light fluorescence, and the laser output power shows that a better understanding of the kinetics in the discharge-pumped XeCl laser has been achieved. However, some questions regarding the uniqueness of the set of reactions and rate coefficients used in the present kinetics model remain unresolved. Further works in this area are, therefore, recommended.

XIII. METHOD FOR DETERMINATION OF CO-SPECTRAL GAIN AND ABSORPTION COEFFICIENTS IN HIGH-POWER LASERS[†]

(S. C. Lin, S. B. Zhu, Q. H. Lou, and Q. S. He, paper accepted for publication in the Journal of Quantitative Spectroscopy and Radiative Transfer, October 1983; probable publication date: June or July 1984)

Summary

A new method is described for determining the small-signal gain and non-saturable absorption coefficients over the same spectral region for high-power lasers. Preliminary tests of this method on the discharge-pumped XeCl excimer laser have yielded $B\,^2\Sigma \rightarrow X\,^2\Sigma$ gain coefficients which are comparable to those observed in other experiments under similar excitation conditions. However, the absorption coefficient is found to be a high and nearly constant fraction ($\sim 1/4$) of the gain. This result suggests that all of the absorption processes are due to excited species, including XeCl $B\,^2\Sigma$.

[†]Work supported, in part, by the Defense Advanced Research Projects Agency under Contract N00014-76-C-0116 monitored by the Office of Naval Research, and by the National Science Foundation under Grant CPE82-19521.

1. INTRODUCTION

The small-signal gain and non-saturable absorption coefficients, $g(\lambda)$ and $\kappa(\lambda)$, of the excited medium are important parameters which govern the mode buildup time, saturation intensity, and ultimate optical extraction efficiency of high-power laser oscillators and amplifiers.[1] The simplest and most commonly used method for measuring both $g(\lambda)$ and $\kappa(\lambda)$ is a transmission experiment in which a low-intensity probe beam of sufficiently narrow spectral width $\Delta\lambda$ at the desired wavelength λ is sent through a homogeneously excited medium of length L_m. Comparison between the transmitted beam intensity $I_2(\lambda)$ and the initial probe beam intensity $I_1(\lambda)$ yields the net gain coefficient

$$G(\lambda) \equiv g(\lambda) - \kappa(\lambda) = \frac{1}{L_m} \ln[I_2(\lambda)/I_1(\lambda)]. \qquad (1)$$

This net gain coefficient may be identified with $g(\lambda)$ or $-\kappa(\lambda)$ only when one or the other coefficient is negligibly small in absolute value.

In the study of laser mode buildup and saturation in high-gain systems, one is particularly interested in knowing the values of $g(\lambda)$ and $\kappa(\lambda)$ at or near the center wavelength λ_o of the relevant atomic line or rotational lines within the strongest emission bands. To determine $g(\lambda_o)$ from the measured value of $G(\lambda_o)$, one must know $\kappa(\lambda_o)$. Direct measurement of $\kappa(\lambda_o)$ in the presence of gain is generally difficult or impossible. Accordingly, past measurement of $\kappa(\lambda)$ have usually been confined to spectral regions somewhat removed from the peaks of the laser emission spectrum,[2, 3] and the value of $\kappa(\lambda_o)$ could only be inferred by interpolation or extrapolation.

In the present paper, a new method is described for determining $g(\lambda)$ and $\kappa(\lambda)$ at the same value of λ, which may include the peak-gain wavelength λ_o. This method appears to work particularly well for high-gain systems, such as the rare gas halogen excimers,[4] where the laser mode buildup time in small optical cavities can be made very short in comparison with the total excitation time.[5] Some preliminary results obtained for the discharge-pumped XeCl excimer laser using this method are presented and discussed.

2. DESCRIPTION OF THE METHOD

The method involves the combination of two separate measurements carried out under otherwise identical excitation conditions. As illustrated schematically in Fig. 1, the first is a measurement of the net gain coefficient $G(\lambda)$ at the desired wavelength $\lambda = \lambda_o$ in accord with Eq. (1) using a probe beam which can be generated from a laser oscillator at output wavelength λ_o through appropriate attenuators or from an incoherent radiation source through appropriate narrow-band filters and collimators. The second is a measurement of the saturated laser oscillator power output, P_L, from the excited medium over the same wavelength λ_o and wavelength interval $\Delta\lambda$ as chosen for the probe beam, at two or more different values of the cavity loss coefficient α_c. According to theories of laser oscillators and amplifiers,[6,7] the saturation intensity for a homogeneously-broadened line undergoing laser oscillation at wavelength λ_o is proportional to $[g(\lambda_o)/\alpha(\lambda_o)] - 1$, where $\alpha(\lambda_o) \equiv \kappa(\lambda_o) + \alpha_c$ is the equivalent total

(i) MEASUREMENT OF NET SPECTRAL GAIN

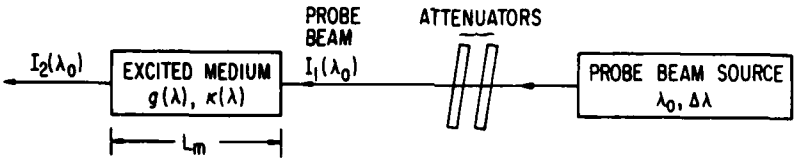

(ii) MEASUREMENT OF SATURATED LASER OSCILLATOR POWER OUTPUT

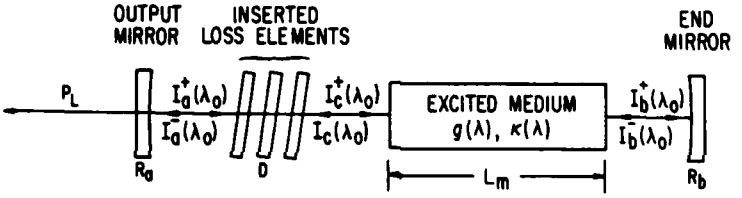

Fig. 1 (XIII) Essential elements of the two independent measurements used in the proposed method for determining the small-signal gain coefficient $g(\lambda)$ and the non-saturable absorption coefficient $\kappa(\lambda)$ at the same wavelength, $\lambda = \lambda_o$.

loss coefficient per unit length of the excited medium at the selected wavelength λ_o. Combination of the two measurements should provide a sensitive and unambiguous method for determining $g(\lambda_o)$ and $\kappa(\lambda_o)$.

To derive some approximate formulae for explicit determination of $g(\lambda_o)$ and $\kappa(\lambda_o)$ from the two measurements, we follow the practice of treating the laser oscillator mode buildup and saturation problems as being equivalent to those of quasi-one-dimensional beam propagation through a semi-infinite, periodic structure.[8-10] The transmission properties of the structure are to be determined by the optical properties of the cavity mirrors and of the intervening media. Referring to Fig. 1(ii), let L be the total optical path length between the output coupling mirror of power reflectance R_a and the end mirror of power reflectance R_b; L_a the path length between R_a and the inserted loss elements of total optical density D; L_c the path length between D and the excited medium of length L_m; and L_b the path length between the end of L_m and R_b. For simplicity, we assume that, through proper choice of geometrical configuration, the beam waves[9] corresponding to the dominant modes of the cavity are of nearly-constant cross section and have negligible diffraction losses.[11] Other minor losses, such as atmospheric absorption and scattering and losses due to the end windows which confine the excited medium, may also be neglected. Within such a cavity, the saturation (steady-state) intensities of the two counter-propagating beam waves within the path segments L_a, L_b, L_c will be piecewise uniform and simply related, i.e.,

$$I_a^+ = I_a^- R_a \,, \tag{2}$$

$$I_b^- = I_b^+ R_b \,, \tag{3}$$

$$I_c^+ / I_a^+ = I_a^- / I_c^- = 10^{-D} = \exp(-2.303\,D) \,, \tag{4}$$

$$I_b^+ / I_c^+ = I_c^- / I_b^- = \exp(G_s L_m) \,, \tag{5}$$

where

$$G_s \equiv g_s - \kappa_s \tag{6}$$

is the net gain coefficient at saturation. All spectral intensities, gain and loss coefficients are evaluated at the same selected wavelength λ_o. The value of G_s is governed by the steady-state condition that the roundtrip gain must be equal to the roundtrip loss so that

$$G_s L_m = 2.303\,D + \ln[\,1/\sqrt{R_a R_b}\,] \,. \tag{7}$$

It should be noted that G_s in Eqs. (5) and (7) represents some averaged value of the saturated net gain coefficient, which actually depends on the detailed distribution of the saturated beam wave intensities $I^+(z)$ and $I^-(z)$ along the optical path length z within L_m. These intensities, in turn, can be determined by a saturation analysis similar to that described by Rigrod[12] provided that the dependence of G_s on total beam intensity (i.e., the sum of I^+ and I^-) is known. However, in some excited media such as the rare gas halogen plasma,[4] the absorption coefficient $\kappa(\lambda_o)$ may involve unknown excited species and even absorption by the excimer at the upper laser state

so that the functional relation between G_s and $(I^+ + I^-)$ cannot be predetermined. Accordingly, we treat the detailed distributions of beam wave intensities within L_m as unknowns but assume that the averaged value of $(I^+ + I^-)$ is approximately the same as the algebraic mean of its endpoint values, $(I_b^+ + I_b^- + I_c^+ + I_c^-)/2$. Similar approximation can also be made for the averaged beam wave intensities within the inserted loss elements D. The averaged saturation intensity of the beam wave over one roundtrip path length of the optical cavity, $2L \equiv 2(L_a + L_b + L_c + L_d + L_m)$, is then

$$I_s = \frac{1}{2L}\left[\left(L_a + \frac{L_d}{2}\right)(I_a^+ + I_a^-) + \left(L_b + \frac{L_m}{2}\right)(I_b^+ + I_b^-) + \left(L_c + \frac{L_d}{2} + \frac{L_m}{2}\right)(I_c^+ + I_c^-)\right]. \tag{8}$$

With the help of Eqs. (2) through (7), this averaged intensity can be related to the beam wave intensity at the output coupling mirror, I_a^-, which determines the laser oscillator output power P_L, viz.,

$$I_s = \{\xi + \eta[\exp(2.303D) + R_a \exp(-2.303D)]\} I_a^-, \tag{9}$$

where ξ and η are known geometrical parameters of the optical cavity defined by

$$\xi \equiv [(2L_a + L_d)/4L](1 + R_a) + [(2L_b + L_m)/4L](\sqrt{R_a/R_b} + \sqrt{R_a R_b}), \tag{10}$$

$$\eta \equiv (2L_c + L_d + L_m)/4L. \tag{11}$$

The roundtrip-averaged saturation intensity I_s for the beam wave within the oscillator [Eq. (9)] can now be equated to the limiting intensity I_ℓ for a long laser pulse of the same selected wavelength, $\lambda = \lambda_o$, and bandwidth, $\Delta\lambda$, propagating in a semi-infinite, homogeneously-excited medium of the same small-signal gain coefficient $g(\lambda)$. However, the equivalent non-saturable absorption coefficient $\alpha(\lambda)$ must include a distributed loss term due to the inserted elements D and the cavity mirrors R_a, R_b, of the oscillator, so that

$$\alpha(\lambda) = \kappa(\lambda) + \frac{1}{L_m}\left[2.303\,D + \ln\left(\frac{1}{\sqrt{R_a R_b}}\right)\right]. \qquad (12)$$

If $\Delta\lambda$ is much narrower than the spectral width of the gain profile $g(\lambda)$ and the laser transition involves only two discrete quantum states in a homogeneously-broadened excited medium, the limiting intensity I_ℓ should be quite close to that derived by Icsevgi and Lamb[7] for a monochromatic wave propagating in such a two-level excited medium. The limiting spectral intensity $I_\ell(\lambda)$, when expressed in terms of radiative power flux per unit area per unit wavelength interval about λ, in the mks system of units, is then

$$I_\ell(\lambda) = \frac{c\,\epsilon_o h^2 \gamma_{ul} \gamma}{8\pi^2 p^2 \Delta\lambda}\left[\frac{g(\lambda) - \alpha(\lambda)}{\alpha(\lambda)}\right]\left[\mathcal{L}(\nu - \nu_o)\right]^{-1}. \qquad (13)$$

In Eq. (13), c is the velocity of light in vacuum, $\epsilon_o = 8.85 \times 10^{-12}$ farad/m is the permittivity of free space, h is Planck's constant, γ_{ul} is the decay constant for the dipole moment of the two-level atom involved in the laser

transition $u \rightarrow l$, $\wp^2$ is the squared-amplitude of the matrix element of this dipole moment, γ is the reciprocal of the mean life time of the upper and lower quantum states, u, l, including the shortening effects due to collisional quenching, and

$$\mathcal{L}(\nu - \nu_o) = \gamma_{ul}^2 \left[(\nu - \nu_o)^2 + \gamma_{ul}^2 \right]^{-1} \tag{14}$$

is a dimensionless Lorentzian function with $\nu \equiv c/\lambda$, and $\nu_o \equiv c/\lambda_o$.

If the laser transition involves molecular bands as in the rare gas halogen excimers,[4] the propagating beam may include many laser lines oscillating simultaneously among many pairs of vibrational-rotational quantum states. In order to make use of analytical results which have been derived only for the two-level system,[7] we must make an additional simplifying assumption that each saturated laser line within the oscillator or within the propagating pulse involves only one pair of vibrational-rotational states in the excited molecular system, and the relative population of such pairs of states is governed only by collisional effects. For mathematical convenience, we further assume that each saturated line oscillates at the respective line-center frequency ν_o of the corresponding pair of states, and that the values of γ_{ul}, γ, and $\wp^2$ are all approximately the same for all of the pairs of states involved. Let A_L be the cross-sectional area of the propagating beam and N_L be the effective number of saturated laser lines in the beam. The total saturated power of the propagating beam is then

$$P_B = N_L A_L I_\ell(\lambda_o)\Delta\lambda = N_L A_L \Phi \left[\frac{g(\lambda_o) - \alpha(\lambda_o)}{\alpha(\lambda_o)} \right], \tag{15}$$

where $\Phi \equiv c\epsilon_o h^2 \gamma_{ul} \gamma / 8\pi^2 \wp^2$. The saturated laser oscillator power output, on the other hand, is given by $P_L = T_a P_a^-$, where $T_a \approx 1 - R_a$ is the transmittance of the output coupling mirror and P_a^- is the incident beam power at the same mirror. This beam power is related to the roundtrip-averaged beam power within the oscillator cavity, P_s, and the intensity ratio defined by Eq. (9), such that $P_s / P_a^- = I_s / I_a^-$. By identifying P_s with the saturated beam power P_B given by Eq. (15), we obtain

$$P_L = \frac{N_L A_L \Phi T_a [G(\lambda_o) - \kappa_{ab} - \kappa_i] / [\kappa(\lambda_o) + \kappa_{ab} + \kappa_i]}{\xi + \eta [\exp(2.303 D) + R_a \exp(-2.303 D)]} . \qquad (16)$$

Here, $G(\lambda_o)$ and $\kappa(\lambda_o)$ denote, as before, the net small-signal gain and non-saturable absorption coefficients for the excited medium at the corresponding line-center wavelength (or wavelengths), $\kappa_{ab} \equiv [\ln(1/\sqrt{R_a R_b})] / L_m$ is the equivalent loss per unit gain length due to the two cavity mirrors, and $\kappa_i \equiv 2.303 D / L_m$ is the equivalent loss per unit gain length due to the inserted loss elements [see Eq. (12)]. The saturated laser oscillator power output in the absence of any inserted loss elements is, therefore,

$$P_{L0} = \frac{N_{L0} A_L \Phi T_a [G(\lambda_o) - \kappa_{ab}] / [\kappa(\lambda_o) + \kappa_{ab}]}{\xi + \eta (1 + R_a)} . \qquad (17)$$

A different symbol N_{L0} has been introduced here to allow for the fact that the number of saturated laser lines, which contributed to the measured value of P_{L0}, may or may not be the same as N_L, which contributed to the measured value of P_L under otherwise identical excitation conditions. The ratio

between the two values of the oscillator power output is, therefore,

$$\Gamma \equiv \frac{P_{L0}}{P_L} = \frac{\Lambda N_{L0}[G(\lambda_o) - \kappa_{ab}][\kappa(\lambda_o) + \kappa_{ab} + \kappa_i]}{N_L[G(\lambda_o) - \kappa_{ab} - \kappa_i][\kappa(\lambda_o) + \kappa_{ab}]} . \qquad (18)$$

The factor $\Lambda \equiv \left|\xi + \eta[\exp(2.303D) + R_a \exp(-2.303D)]\right| / [\xi + \eta(1 + R_a]$ in Eq. (18) is generally very close to unity for small values of D. Assuming $N_{L0}/N_L \approx 1$, we obtain from rearrangement of Eq. (18) the following approximate formula for explicit determination of $\kappa(\lambda_o)$ from the experimental values of $G(\lambda_o)$ and Γ for any fixed set of excitation conditions using a suitably chosen (non-zero) value of $\kappa_i \equiv 2.303D/L_m$:

$$\kappa(\lambda_o) = [(\kappa_{ab} + \kappa_i)F - \kappa_{ab}\Gamma]/(\Gamma - F), \qquad (19)$$

where $F \equiv \Lambda[G(\lambda_o) - \kappa_{ab}]/[G(\lambda_o) - \kappa_{ab} - \kappa_i]$. The co-spectral small-signal gain coefficient can subsequently be determined from

$$g(\lambda_o) \equiv G(\lambda_o) + \kappa(\lambda_o). \qquad (20)$$

It should be noted that an expression similar to Eq. (18) for relating the ratio of the two saturated laser oscillator power outputs can also be derived from Rigrod's analysis of the saturation effects in high-gain lasers,[12] but using the method suggested by Champagne et al[13, 14] for inclusion of the absorption term due to the excited medium in an approximate manner. Rigrod[12] has shown that, for a laser oscillator consisting of a homogeneously-broadened excited medium of small-signal gain coefficient g_o and length L bounded

at the two ends by a pair of cavity mirrors of reflectances r_1 and r_2, the steady-state intensities of the two out-going beam waves I_1^-, I_2^+, directed at mirror r_1 and r_2, respectively, are related to the referenced saturation intensity I_o by

$$I_1^- = (r_2/r_1)^{1/2} I_2^+ = \frac{(r_2)^{1/2}[\, g_o L + \ln(r_1 r_2)^{1/2}\,]}{[(r_1)^{1/2} + (r_2)^{1/2}][\, 1 - (r_1 r_2)^{1/2}\,]} I_o \,. \qquad (21)$$

Derivation of this equation was based on the assumptions that the excited medium is non-absorbing, and that the local saturated gain coefficient $g(z)$ is related to g_o and the local beam intensities $I^+(z)$, $I^-(z)$, such that $g(z) = g_o / \{\, 1 + [\, I^+(z) + I^-(z)\,]/I_o \,\}$. The referenced intensity I_o, therefore, is the total intensity at which $g(z) = g_o/2$. According to Eq. (21), the out-going beam wave intensities I_1^-, I_2^+, would be infinite if both mirrors were perfect reflectors (i.e., $r_1 = r_2 = 1$). The approximate method suggested by Champagne et al [13, 14] for modification of Eq. (21) to accommodate a finite, non-saturable absorption coefficient κ in the excited medium was to lump the distributed absorption losses through the medium as additional discrete fractional power losses at the two mirrors. By adopting this approximate method to the oscillator arrangement illustrated in Fig. 1(ii), we may similarly lump the single-pass absorption loss through the medium, $[\, 1 - \exp(-\kappa L_m)\,]$, at the out-going end of the medium for each of the two counter-propagating beam waves. The emerging beam intensities, I_c^- and I_b^+, at the two ends of the excited medium are then related to the lossless beam intensities I_1^-, I_2^+, such that

$$I_c^- / I_1^- = I_b^+ / I_2^+ = \exp(-\kappa L_m). \qquad (22)$$

The effective reflectances seen by the two out-going beam waves, I_1^- and I_2^+, counting all of the optical components shown in Fig. 1(ii), are, therefore, $r_1 = R_a \exp(-\kappa L_m - 4.606 D)$ and $r_2 = R_b \exp(-\kappa L_m)$, respectively. Substituting these into Eq. (21) and using symbols already introduced, with the abbreviations $G \equiv g_o - \kappa(\lambda_o)$, $\kappa \equiv \kappa(\lambda_o)$, we obtain

$$I_a^- = \frac{\sqrt{R_b}\,(G - \kappa_{ab} - \kappa_i) L_m \exp[-(\kappa + \kappa_i) L_m]\, I_o}{[\sqrt{R_a} \exp(-\kappa_i L_m) + \sqrt{R_b}]\{1 - \exp[-(\kappa + \kappa_{ab} + \kappa_i) L_m]\}}. \qquad (23)$$

The ratio of laser oscillator power outputs defined earlier, $\Gamma \equiv P_{L0} / P_L = I_a^-(\kappa_i = 0) / I_a^-(\kappa_i \neq 0)$, is, accordingly,

$$\Gamma = \frac{\Lambda'\,(G - \kappa_{ab})\{1 - \exp[-(\kappa + \kappa_{ab} + \kappa_i) L_m]\}}{(G - \kappa_{ab} - \kappa_i)\{1 - \exp[-(\kappa + \kappa_{ab}) L_m]\}}. \qquad (24)$$

Here, the factor $\Lambda' \equiv [\sqrt{R_a} + \sqrt{R_b} \exp(-\kappa_i L_m)] / (\sqrt{R_a} + \sqrt{R_b})$, although different from the factor Λ in Eq. (18), is again very close to unity at small values of $\kappa_i L_m$. Thus, when the total single-pass loss $(\kappa + \kappa_{ab} + \kappa_i) L_m$ is sufficiently small in comparison with unity, as in the case of the preliminary experiments described below, the exponential factors in Eq. (24) can be approximated by the first two terms of the corresponding power series expansions. The resultant equation then becomes essentially the same as Eq. (18).

3. EXPERIMENTAL ARRANGEMENT

The indicated method has been used in the determination of $g(\lambda_o)$ and $\kappa(\lambda_o)$ for the XeCl $B\,^2\Sigma_{1/2} \rightarrow X\,^2\Sigma_{1/2}$ transitions at $\lambda_o = 307.94$ and 308.19 nm, corresponding to the spectral peaks of the two strongest bands, (0,1) and (0,2), respectively, observed in laser emissions.[15,16] The experimental arrangement for measuring the small-signal net gain coefficient $G(\lambda_o)$ is illustrated in Fig. 2, while the arrangement for measuring P_L at different values of the inserted loss coefficient κ_i is illustrated in Fig. 3.

In the net gain measurement, the excited medium was generated in a very small volume, X-ray preionized pulsed avalanche discharge using dilute Ne/Xe/HCl mixtures at initial gas pressures ranging between 1 and 10 atm. As described in considerable detail in Ref. 5, this small discharge system consisted of a cylindrical discharge chamber of ~ 8 cm inside diameter and 7 cm maximum interior height (chamber 1 in Fig. 2), and a high voltage pulse forming network (PFN). The effective discharge volume and geometry were controlled by the aperture area of the preionizing X-ray flux and the gap spacing between the discharge electrodes. The discharge pulse duration was controlled by the electrical length (two-way propagation time) of the transmission line within the PFN. The self-sustained discharge current, after completion of the avalanche process, was controlled by the initial charged-up voltage V_c on the PFN and the output impedance Z_o of the PFN. The latter was determined by the number of 50Ω coaxial cables (RG-8/U) connected in parallel to form the transmission line. The PFN was initially isolated from the discharge chamber through a self-triggered rail gap switch

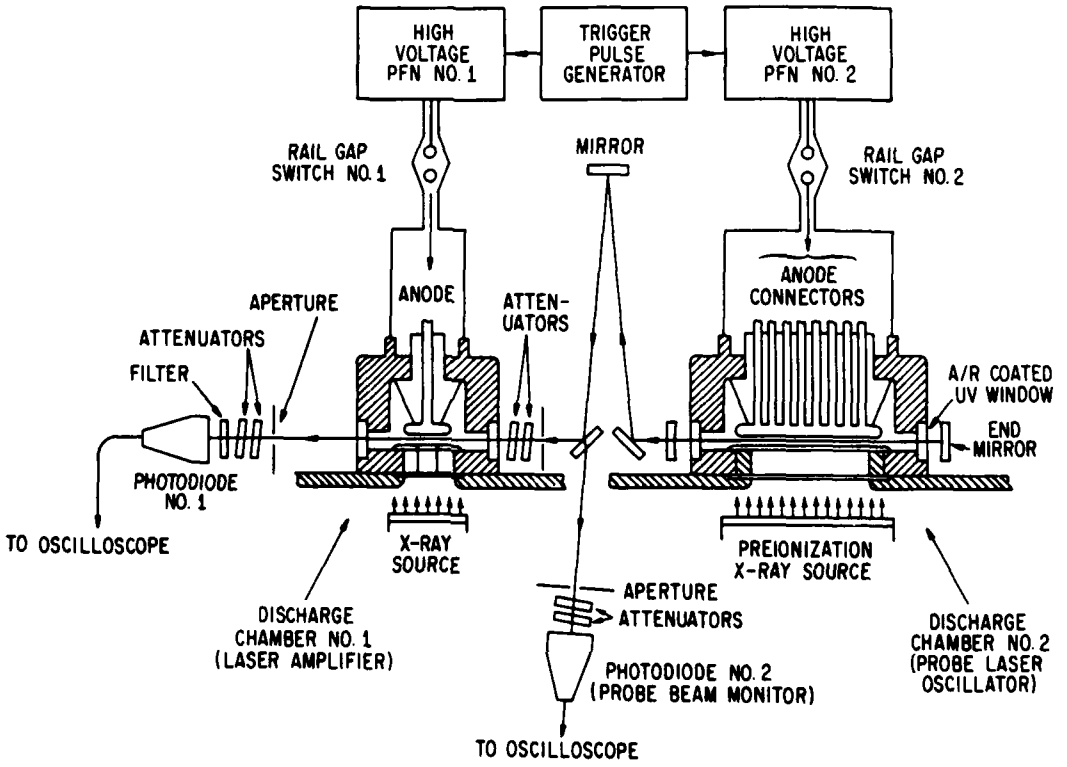

Fig. 2 (XIII) Experimental arrangement for measurement of the small-signal net gain coefficient $G(\lambda) \equiv g(\lambda) - K(\lambda)$ in a pulse-discharge-excited medium. By using the same gas mixture in both of the discharge chambers and a broad-band oscillator cavity, the probe beam wavelengths λ_o were automatically tuned to those corresponding to the strongest laser transitions in the excited medium.

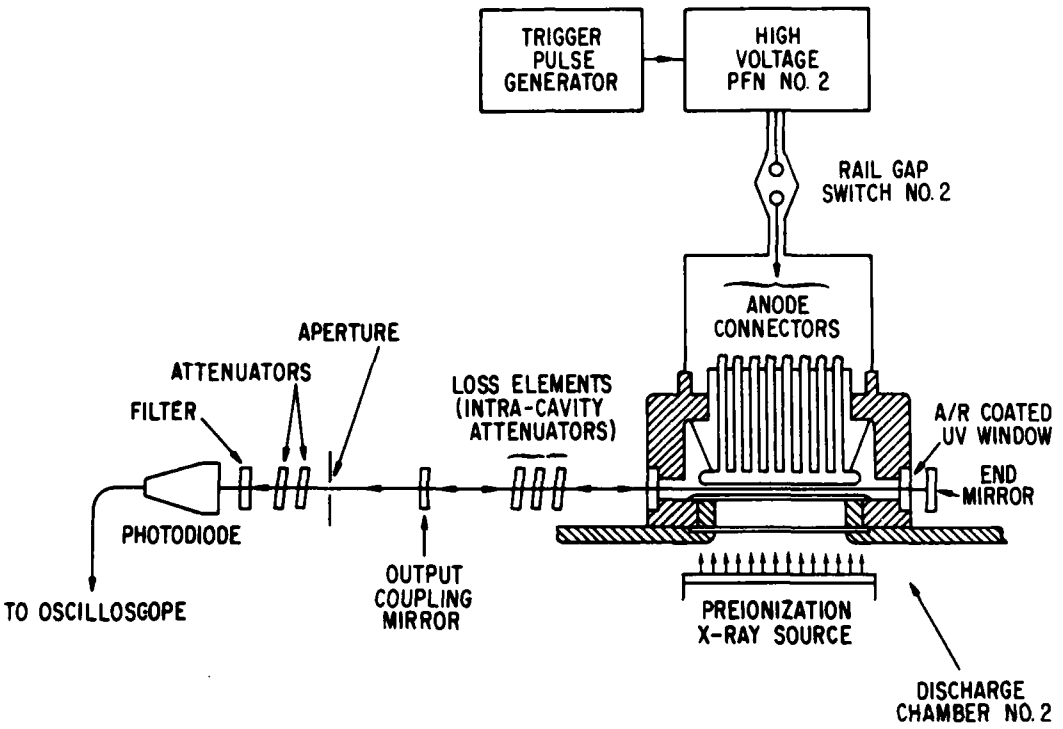

Fig. 3 (XIII) Experimental arrangement for measurement of the saturated power output P_L from a pulse-discharge-excited laser oscillator at different values of the cavity-loss coefficient.

set at a pre-determined value of V_c. As indicated in Fig. 2, the probe beam was a low power XeCl laser generated from another small discharge system of similar design. The second discharge chamber was of a rectangular geometry with elongated electrodes in the direction of the optical axis. The longer usable gain length in the second chamber ($\sim$ 14 cm vs. $L_m \leq 6$ cm in the first chamber) assured that the probe-beam-pulse duration could be made longer than the XeCl B $\rightarrow$ X fluorescence duration in the first chamber through proper choices of the gas pressure and current density.[5] This longer gain length also allowed the measurement of saturated laser oscillator power to be made over the lower range of value of $G(\lambda_o)$ using the experimental arrangement illustrated in Fig. 3. The two discharge chambers were mounted on the top plate of the low-energy X-ray preionization source[17] through pre-selected aperture openings. The preionization source was synchronously triggered with the pulse-charging circuits within the two PFNs connected to the discharge chambers through adjustable time delays. Both discharge chambers were sealed by anti-reflection-coated fused silica windows of 3.81 cm diameter, 0.95 cm thickness, and 0.001 initial (clean) reflectance over the spectral range $295 < \lambda < 305$ nm.[18]

The optical cavities for generating the XeCl laser probe beam and for carrying out the measurement of saturated XeCl laser oscillator power output using either discharge chamber 1 or 2 were formed by dielectric-coated mirrors of 3.81 cm diameter and 10 m concave radius of curvature on fused silica substrates. The end mirror was a nearly total reflector with power reflection coefficient $R_b \geq 0.99$ (as rated by the supplier, CVI Laser Corporation)

at $\lambda \approx 308$ nm. The output coupling mirror was a partial reflector with an estimated absorption loss coefficient of ~ 0.01 and a power reflection coefficient $R_a = 0.98$. The distance between mirror surfaces was set at 30 cm for probe-beam generation and at 34 cm for measurement of P_L when discharge chamber 2 was used. For measurement of P_L using the shorter chamber, the mirror separation distance was reduced to 24 cm.

The gap spacing between discharge electrodes was kept constant at 1 cm for both discharge chambers. The X-ray aperture opening for chamber 2 was 14 cm long and 0.5 cm wide so that the effective discharge volume was $14 \times 0.5 \times 1$ cm^3 in all of the experiments. For the shorter chamber, the aperture opening was set at 5.5×0.5 cm^2 when the chamber was used for measurement of P_L. During the measurement of $G(\lambda_o)$, the aperture opening was set at 4×1 cm^2 to ensure that the excited medium in chamber 1 was at least a factor of 2 wider than the probe beam emerging from the output coupling mirror of the laser oscillator at chamber 2. The probe beam out of the oscillator, which was about 0.5 cm wide and a factor of 100 below the saturation intensity inside the optical cavity due to the $\sim 1\%$ transmittance of the output coupling mirror, was further attenuated by a number of mirrors and attenuators before being admitted into chamber 1 (Fig. 2). The resultant low intensity of the probe beam thus assured that the net gain $G(\lambda_o)$ measured in accord with Eq. (1) corresponded to the small-signal net gain.

In the experimental arrangement for measuring the saturated laser oscillator power output P_L at different values of the inserted loss coefficient κ_i (Fig. 3), the inserted loss elements were uncoated fused silica flats of

approximately 1 mm thickness placed between the output coupling mirror and the discharge chamber window. These uncoated flats were slightly tilted to keep the secondary reflections from reaching the end mirrors on the other side of the chamber. The required tilt angle was so small ($\sim 2^{\circ}$) that the single-pass transmission loss through each flat was approximately twice the normal reflection coefficient $|(n_2 - n_1)/(n_2 + n_1)|^2$ at the air-quartz interface for all polarization angles. Using known values for the refractive index of air ($n_1 = 1.00029$) and of fused quartz ($n_2 = 1.48504$) at $\lambda = 308$ nm,[19] we can deduce a single-pass transmission loss of about 0.0761 for each quartz flat. The optical density for each inserted loss element was, accordingly, $D \approx 0.0761/2.303 \approx 0.033$.

4. PRELIMINARY RESULTS

In Fig. 4, we show some typical oscillographic traces of the voltage and current across the discharge electrodes, the XeCl $B\,^2\Sigma_{1/2} \rightarrow X\,^2\Sigma_{1/2}$ fluorescence (spontaneous emission) intensity, and the XeCl laser oscillator power output at $\lambda \approx 308$ nm observed in the small volume discharge using an Ne:Xe:HCl = 9923:70:7 mixture at two different values of the total gas pressure p. These were obtained from the shorter chamber driven by a 2-cable transmission line in the PFN, but oscillograms taken from the other chamber at comparable discharge conditions looked quite similar. Here, the electrical length of the transmission line was 200 nsec and the discharge cross-section (X-ray aperture) was 4×0.5 cm^2. At p = 3 atm, the avalanche process progressed rapidly after rail-gap switching at t = 0 and was

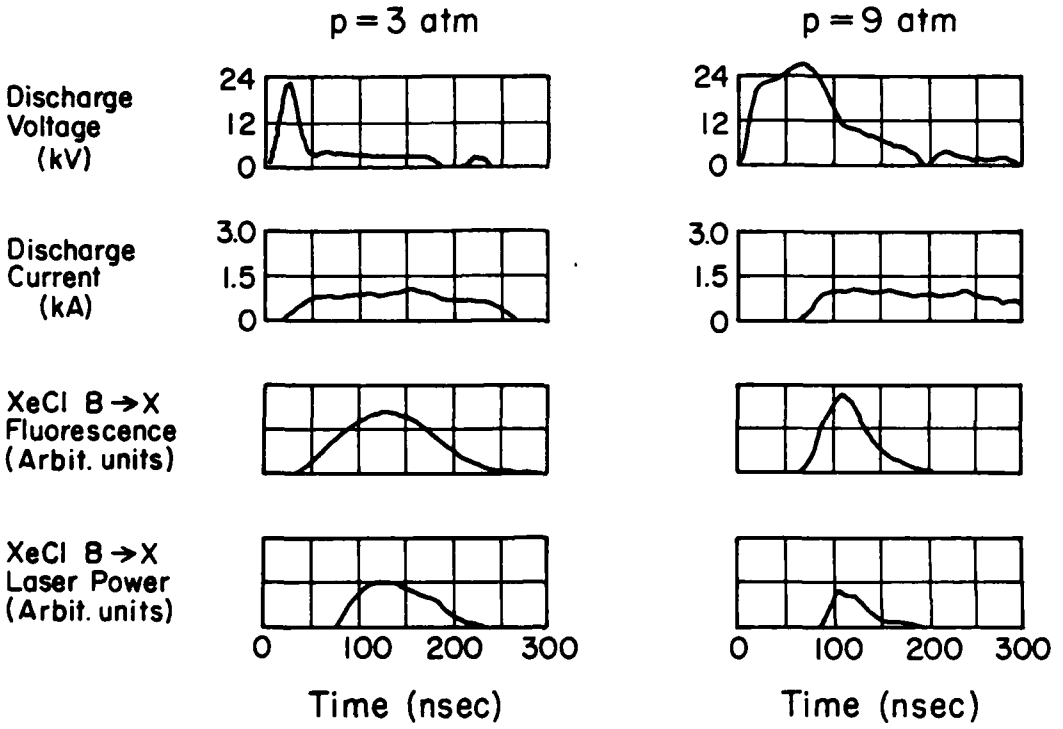

Fig. 4 (XIII) Typical waveforms of the discharge voltage, discharge current, XeCl B → X fluorescence intensity, and laser oscillator power output observed in a 4 x 0.5 x 1 cm^3 volume discharge using an Ne : Xe : HCl = 9923 : 70 : 7 mixture at two different values of the total gas pressure p. The discharge was driven by a transmission line PFN of 25 Ω output impedance, 200 nsec electrical length, and 26 kV pulse-charged voltage.

completed within a time period of about 50 nsec, as indicated by the onset point of a nearly constant self-sustaining voltage $V_{ss} \approx 2.5$ kV and current $I_{ss} \approx 0.8$ kA/cm^2. At p = 9 atm, the peak overvoltage ratio, $V_c / V_{ss} \approx 2$, was somewhat marginal so that it took nearly 100 nsec to complete the electron avalanche. As noted previously,[5] the observed XeCl B → X fluorescence pulse duration was significantly shorter than the ~ 200 nsec duration of the discharge current pulse. The fluorescence pulse duration also tended to decrease with increasing gas pressure and current density. The laser pulse was always somewhat shorter in duration than the corresponding fluorescence pulse and varied with the gas pressure and current density in a similar manner.

In Fig. 5, we show some typical densitometer records of the XeCl B → X fluorescence and laser emission spectra in the vicinity of λ = 308 nm. These spectra were taken under discharge conditions quite similar to those indicated for Fig. 4 during an earlier experiment using chamber 1.[20] The spectral images were recorded in the second-order on Polaroid Type 665 film through the sampling camera on a Spex 1401 double-grating spectrometer of 3/4 m focal length and 2 mm/nm dispersion at λ = 616 nm. Wavelength calibration was provided by the first-order spectrum of a low-pressure neon lamp recorded on the same film. The densitometer traces were generated from the spectral images on the negative film using a Jarrell-Ash Model 23-100 scanning microphotometer. The laser-emission intensity appeared to be concentrated in two broad lines with spectral peaks located at λ_o = 307.94 and 308.19 nm, respectively. These spectral peaks are

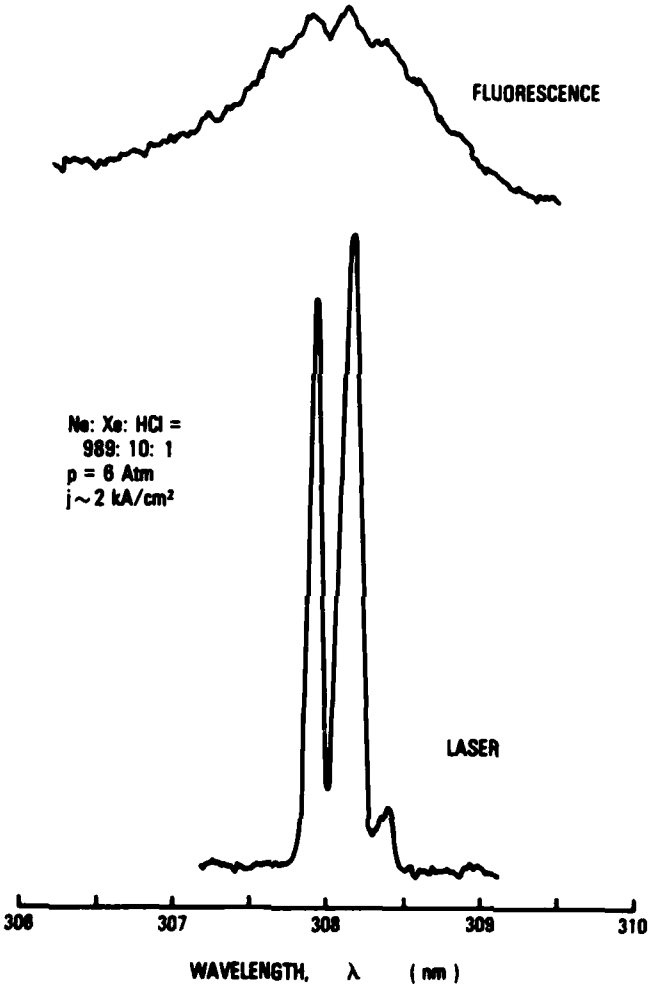

Fig. 5 (XIII) Typical densitometer records of the XeCl B → X fluorescence and laser emission spectra taken from a ~ 200 nsec pulse discharge of $4 \times 0.5 \times 1$ cm^3 volume using an Ne : Xe : HCl = 989 : 10 : 1 mixture at p = 6 atm and j ~ 2 kA/cm^2. The relationship between image density and spectral intensity is roughly logarithmic so that the observed laser-oscillator power output was actually concentrated around the two spectral peaks at λ_o = 307.94 and 308.19 nm, corresponding to the strongest transitions within the (0, 1) and (0, 2) vibrational bands, respectively.

quite close to the bandheads assigned to the $^{136}Xe^{35}Cl$ B → X (0, 1) transition at 307.953 nm and the B → X (0, 2) transition at 308.204 nm by Sur, Hui, and Tellinghuisen.[16] The two broad laser lines shown in Fig. 5 can, therefore, be identified as laser oscillations associated with the highest-gain rotational lines within the XeCl B → X (0,1) and (0,2) bands, which were not spectrally resolved by the recording instrument and photographic film. As noted by Sur et al,[16] the rotational structures of these bands are complex due to the mixed coupling situation, with strong Hund's case c character in the B state. The spectrum is also highly congested on account of the very small vibrational spacing in the weakly-bound X state. Identification of the various oscillating laser mode lines with individual rotational lines would be difficult even if the laser emission lines were spectrally resolved. In the absence of such an identification, the small-signal gain and non-saturable absorption coefficients for the XeCl B → X (0,1) and (0,2) vibrational bands, as deduced from our preliminary experiments described here, must be treated as some weighted average values over the rotational structures of these two bands. The weighing factors for the various rotational states are not known but can be estimated from the simplifying assumption that the rotational populations within the B($v' = 0$) and X($v'' = 1, 2$) vibrational levels are in quasi-equilibrium at an effective translational-rotational temperature that can be determined from kinetics and energy balance considerations.

In Fig. 6, we show some typical oscillograms of the relative probe-beam intensities before and after amplification by the excited XeCl laser plasma generated in discharge chamber 1 using the experimental arrange-

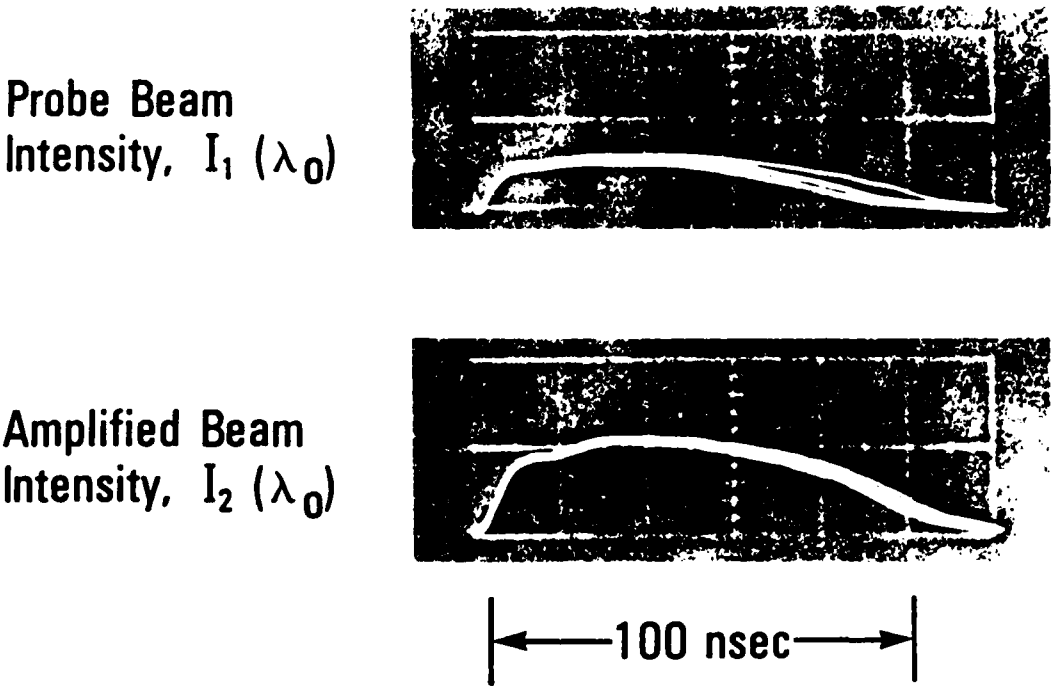

Fig. 6 (XIII) Typical oscillograms from measurement of the small-signal net gain coefficient $G(\lambda) \equiv g(\lambda) - \kappa(\lambda)$ at the XeCl B → X laser oscillation wavelengths $\lambda = \lambda_o \approx 307.94$ and 308.19 nm [Fig. 5 (XIII)] using the experimental arrangement shown in Fig. 2 (XIII). The excited medium was generated in a $4 \times 1 \times 1$ cm^3 volume discharge in chamber 1 using an Ne:Xe:HCl = 9923:70:7 mixture at p = 3 atm and $j \sim 400$ A/cm^2. Each oscillogram was obtained with a cumulative exposure of 5 consecutive pulses.

ment illustrated in Fig. I(i) and in Fig. 2. Each oscillogram was obtained with a cumulative exposure of 5 consecutive pulses to show the magnitude of pulse-to-pulse variations of the detected beam power at photodiode 1 (Fig. 2). The upper oscillogram was obtained by pulsing only the probe beam generator, without any discharge in chamber 1. The lower oscillogram was obtained by simultaneously pulsing both discharge chambers while keeping the probe beam power output (as monitored by photodiode 2) the same as in the upper oscillogram. The use of a single photodiode for measuring both $I_1(\lambda_o)$ and $I_2(\lambda_o)$ thus alleviated the need for cross-calibration of two photodetectors and of the relative losses along two different optical paths. The discharge conditions in chamber 1 were the same as those indicated for the typical oscillographic traces shown in Fig. 4 at $p = 3$ atm, but the oscillograms shown here were taken at 2.5 times higher sweep speed in the internal-trigger mode. It is seen that the amplified beam intensity was now roughly twice the initial probe beam intensity and that the pulse-to-pulse variations of the amplified beam intensity were no greater than those of the initial probe beam intensity.

In Fig. 7, we show some typical oscillograms of the saturated XeCl $B \rightarrow X$ laser oscillator power output P_L, observed at three different values of the inserted loss coefficient κ_i. Each oscillogram was, again, obtained with a cumulative exposure of 5 consecutive pulses. The excited medium for the oscillator was generated in discharge chamber 2 using an Ne : Xe : HCl = 9923 : 70 : 7 mixtures at $p = 2$ atm and $j \sim 400$ A/cm^2. The gain length L_m was 14 cm so that the value of $\kappa_i \equiv 2.303\, D/L_m$, corresponding to

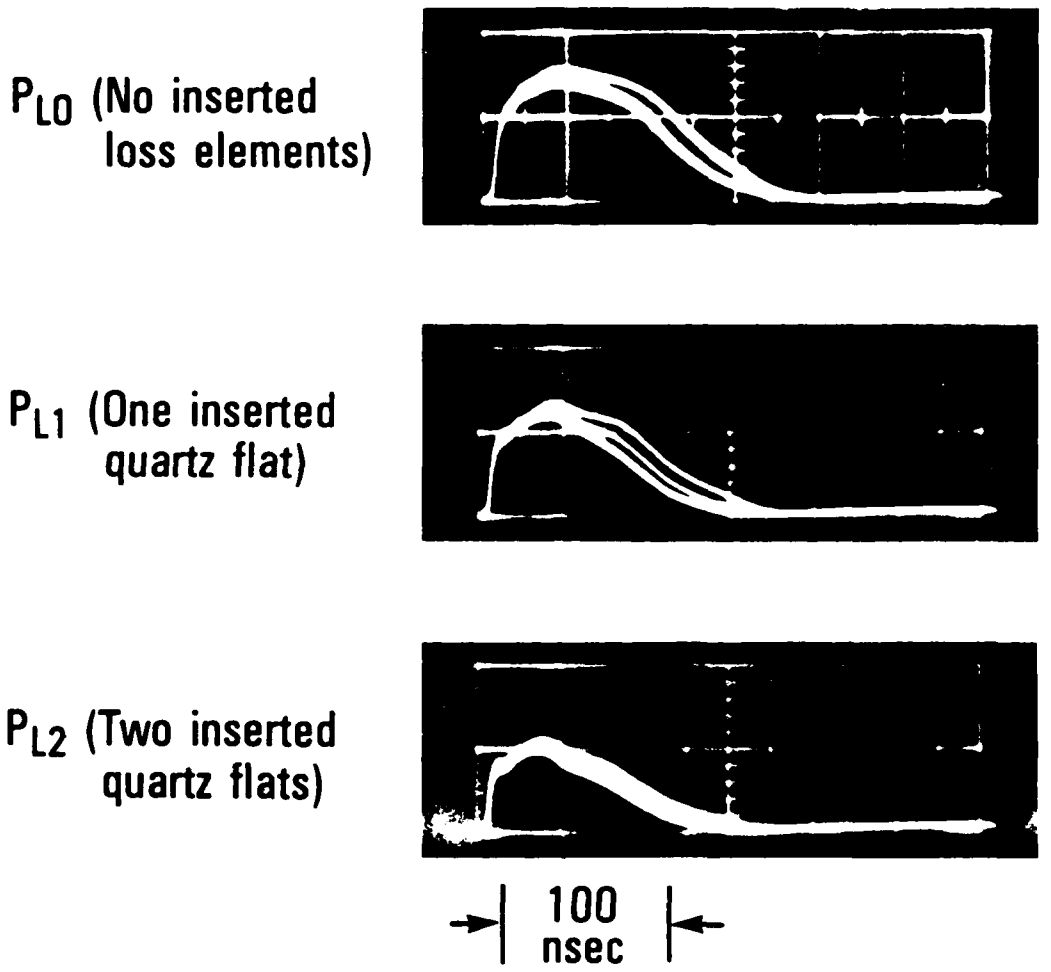

Fig. 7 (XIII) Typical oscillograms from measurement of the saturated laser-oscillator power output P_L at different values of the cavity-loss coefficient under otherwise identical excitation conditions [Fig. 3 (XIII)]. The excited medium was generated in a 14 x 0.5 x 1 cm^3 volume discharge in chamber 2 using an Ne:Xe:HCl = 9923:70:7 mixture at p = 2 atm and j ~ 400 A/cm^2. Each oscillogram was obtained with a cumulative exposure of 5 consecutive pulses.

insertion of one uncoated quartz flat, was 0.00544. The oscilloscope was internally triggered so that all the pulses appeared to rise sharply at the starting point which marked the onset of gain-switching within the laser oscillator. It may be noted that successive insertion of each quartz flat caused an approximately 20% reduction of the mean pulse amplitude and a noticeable change in mean pulse shape. The reduction in pulse amplitude was due to the increased κ_i. The change in mean pulse shape was partly due to shifting of the gain-switching point, and partly due to the nonlinear nature of gain-saturation. It may also be noted that, subsequent to gain-switching, the time scale for significant change of the oscillator power output in each oscillogram ($\sim$ 50 nsec) was quite long in comparison with the roundtrip optical propagation time of the cavity ($\sim$ 2 nsec). Thus, the saturated laser oscillator can be considered as essentially in a quasi-steady-state.

Using Eq. (1) and oscillograms of the type illustrated in Fig. 6, the averaged value of the net gain coefficient over 5 consecutive pulses can readily be determined and plotted as a function of time for each set of preselected experimental conditions. One such plot is illustrated in Fig. 8. Here, the experimental curve refers to the 5-pulse-average value of $G(\lambda_o)$ obtained from the oscillograms shown in Fig. 6. The onset time of the pulse relative to the time of avalanche initiation at $t = 0$ was fixed by examination of externally triggered oscillograms of the type illustrated in Fig. 4.

Summaries of the small-signal gain coefficient $g(\lambda_o)$ and of the co-spectral, non-saturable absorption coefficient $\kappa(\lambda_o)$ corresponding to the XeCl $B \rightarrow X$ (0,1) and (0,2) laser transitions in discharge-excited

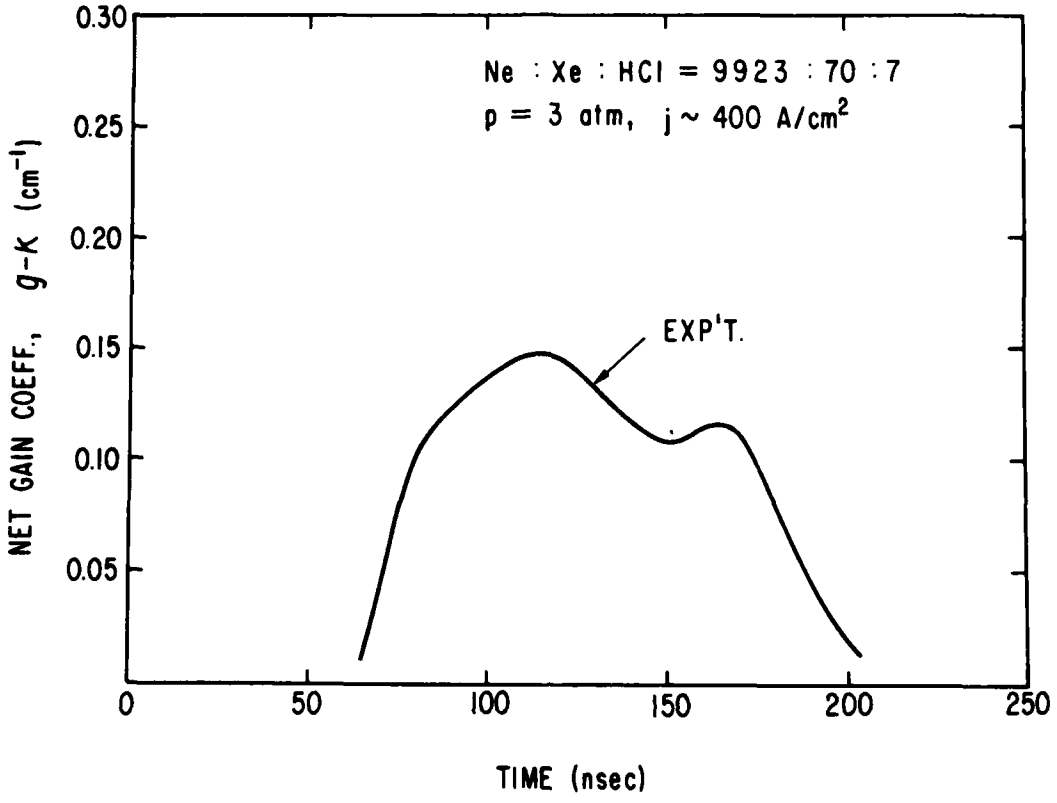

Fig. 8 (XIII) Time history of the small-signal net gain coefficient $G(\lambda_o) \equiv g(\lambda_o) - \kappa(\lambda_o)$ during the pulsed discharge, as deduced from the typical oscillograms shown in Fig. 6 (XIII) using Eq. (1) with $L_m = 4$ cm and instantaneous values of $I_1(\lambda_o)$, $I_2(\lambda_o)$ corresponding to the mean of the 5 consecutive pulses in the respective oscillograms.

Ne/Xe/HCl mixtures over limited ranges of the initial mol ratio, total gas pressure p, and discharge current density j, are presented in Figs. 9 and 10. The approximate values of j indicated for the two sets of experiments refer to the mean current densities deduced from the ratio between the self-sustained discharge current I_{ss} (Fig. 4) and the cross-sectional area of the X-ray aperture. The open points are for $j \sim 200$ A/cm^2 at the three different indicated mixture mol ratios, and the solid points are for $j \sim 400$ A/cm^2 at a single mol ratio Ne:Xe:HCl = 9923:70:7. The experimental values of $\kappa(\lambda_o)$ and $g(\lambda_o)$ were deduced from Eqs. (19) and (20) using the measured values of $G(\lambda_o)$, $P_{L0}(\lambda_o)$, and $P_L(\lambda_o)$ corresponding to either one or two inserted quartz flats in the oscillator cavity. However, instead of using time-averaged values, the experimental points are all based on the peak values of $G(\lambda_o)$, $P_{L0}(\lambda_o)$, and $P_L(\lambda_o)$ in the respective pulses [Figs. 7 and 8]. These peak values, which were found to be in good time-correlation with each other in spite of some uncertainties due to triggering jitters, are more appropriate for the quasi-steady-state conditions assumed in the derivation of Eq. (19) than the time-averaged values.

As shown in Figs. 9 and 10, the experimental values of $g(\lambda_o)$ and $\kappa(\lambda_o)$ appear to be more sensitive to the current density than to the mixture mol ratio and gas pressure. At $j \sim 200$ A/cm^2, $\kappa(\lambda_o)$ appears to be nearly independent of p while $g(\lambda_o)$ shows a weakly rising trend. At $j \sim 400$ A/cm^2, both $\kappa(\lambda_o)$ and $g(\lambda_o)$ show a more rapid rise with increasing p. At fixed values of p and mixture mol ratio, both $g(\lambda_o)$ and $\kappa(\lambda_o)$ appear to increase with j at a rate which is somewhere between the square root and

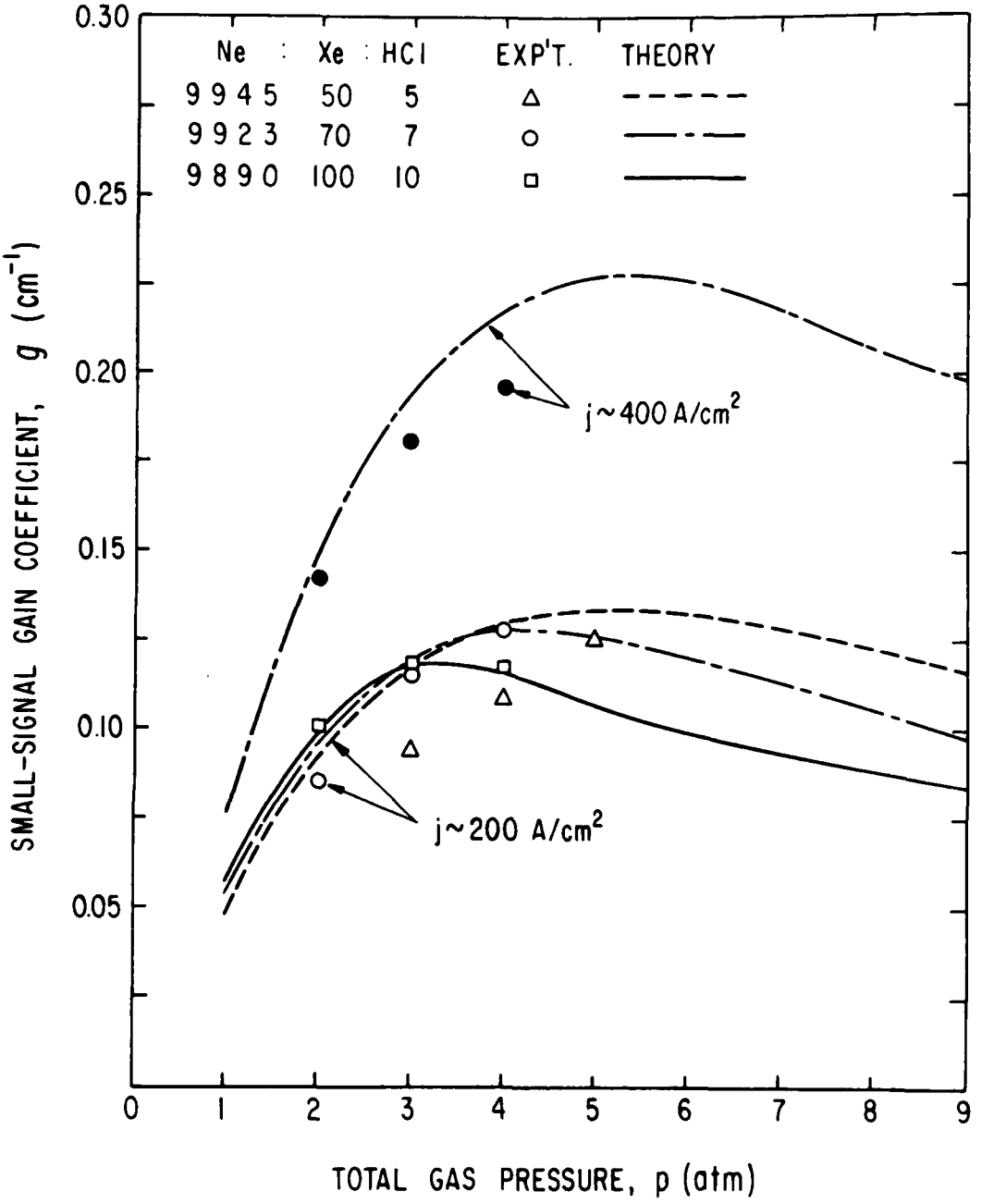

Fig. 9 (XIII) Small-signal gain coefficient $g(\lambda_o)$ at wavelength corresponding to the strongest XeCl B → X laser transitions [Fig. 5 (XIII)], as determined from the peak value of $G(\lambda_o)$ and the concurrent value of $\Gamma \equiv P_{L0}/P_L$ observed in the 200 nsec discharge. The theoretical curves for comparison with the plotted experimental points are based on a simplified quasi-steady-state model of the discharge during the peak-gain period.

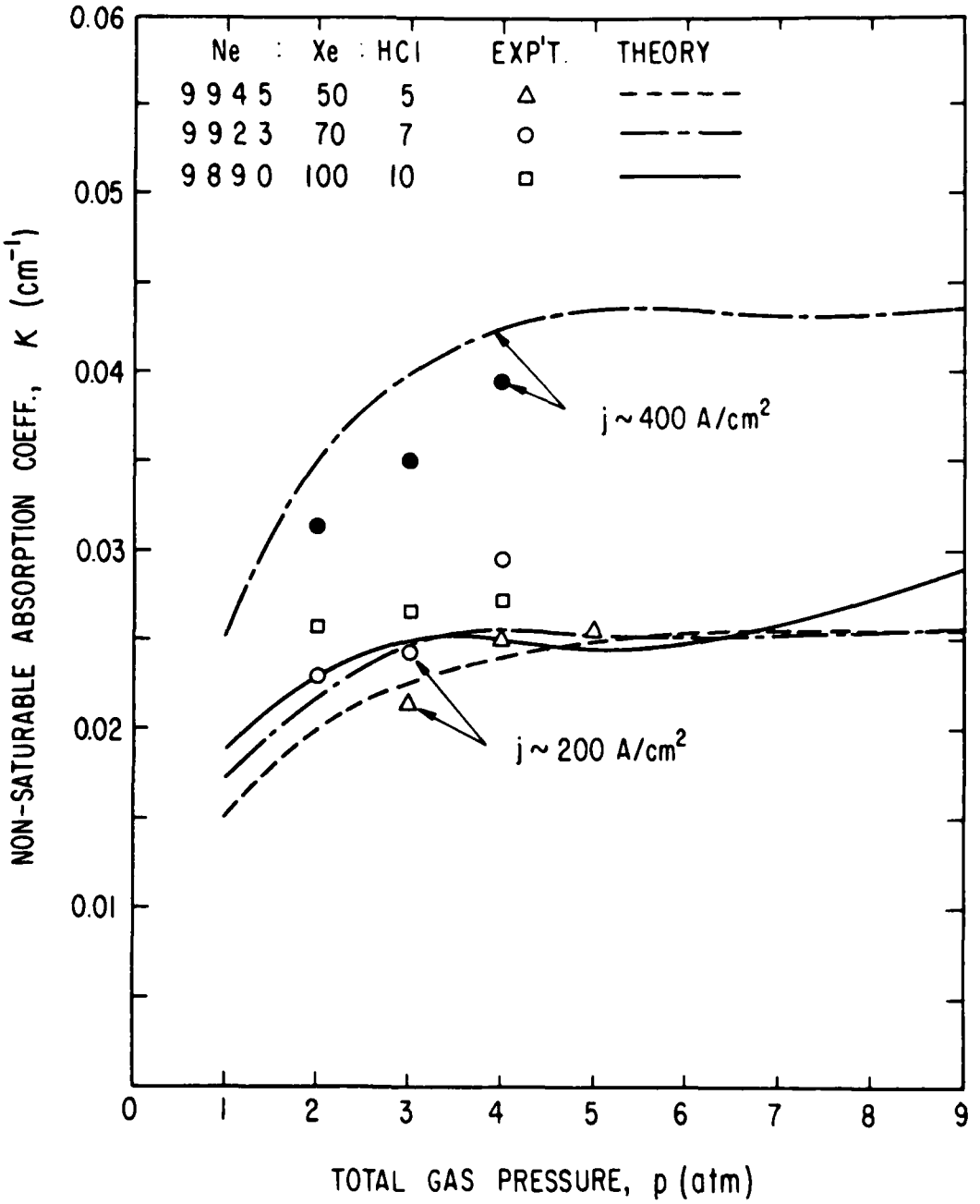

Fig. 10 (XIII) Non-saturable absorption coefficient $\kappa(\lambda_o)$ at wavelength λ_o corresponding to the strongest XeCl B → X laser transitions [Fig. 5 (XIII)] as determined from the peak value of $G(\lambda_o)$ and the concurrent value of $\Gamma \equiv P_{L0}/P_L$ observed in the 200 nsec discharge. The theoretical curves for comparison with the plotted experimental points are based on a simplified quasi-steady-state model of the discharge during the peak-gain period.

the first power of j. The ratio between $g(\lambda_o)$ and $\kappa(\lambda_o)$ is thus nearly independent of the current density. As is shown in Fig. 11, the experimental value of $g(\lambda_o)/\kappa(\lambda_o)$ appears to lie between 3.5 and 5.1 over the entire range of parameters covered in our preliminary experiments.

The net gain coefficient $G(\lambda_o) \equiv g(\lambda_o) - \kappa(\lambda_o)$, as determined from the relatively broad-band experiments at $\lambda_o = 307.94$ and 308.19 nm, which correspond to the spectral peaks of the two strongest laser lines (Fig. 5), is about 0.15 cm^{-1} at p = 4 atm and $j \sim 400$ A/cm^2. This is comparable to the net gain coefficient of 0.18 cm^{-1} observed by Bourne and Alcock[21] in their narrow-band ($\Delta\lambda = 0.00004$ nm) gain measurements using a somewhat different mixture ($Ne:Xe:HCl:H_2 = 3040:20:4:5$) at p = 4 atm and $j \sim 2$ kA/cm^2. The dependence of $g(\lambda_o)$ on gas pressure and on HCl mol fraction observed in our experiments are also in good agreement with those observed by Zheng, Huo, and Wei.[22] The absolute value of $g(\lambda_o)$ observed in our experiments is, however, about a factor of 2 higher at comparable gas pressure and HCl mol fraction. The determination of $g(\lambda_o)$ in Ref. 22 was based on the maximum loss method in which an increasing number of loss elements (dielectric-coated partial reflectors) was inserted into the optical cavity of the XeCl laser oscillator until the oscillation threshold was reached. Data reduction was based on the modified Rigrod equation suggested by Champagne et al,[13,14] as described earlier in Sec. 2. The excited medium was generated in an X-ray preionized discharge of $1.8 \times 1.5 \times 70$ cm^3 effective volume and ~ 70 nsec pulse duration.[23] The gas mixture and pressure were essentially the same as those used in our present experiments,

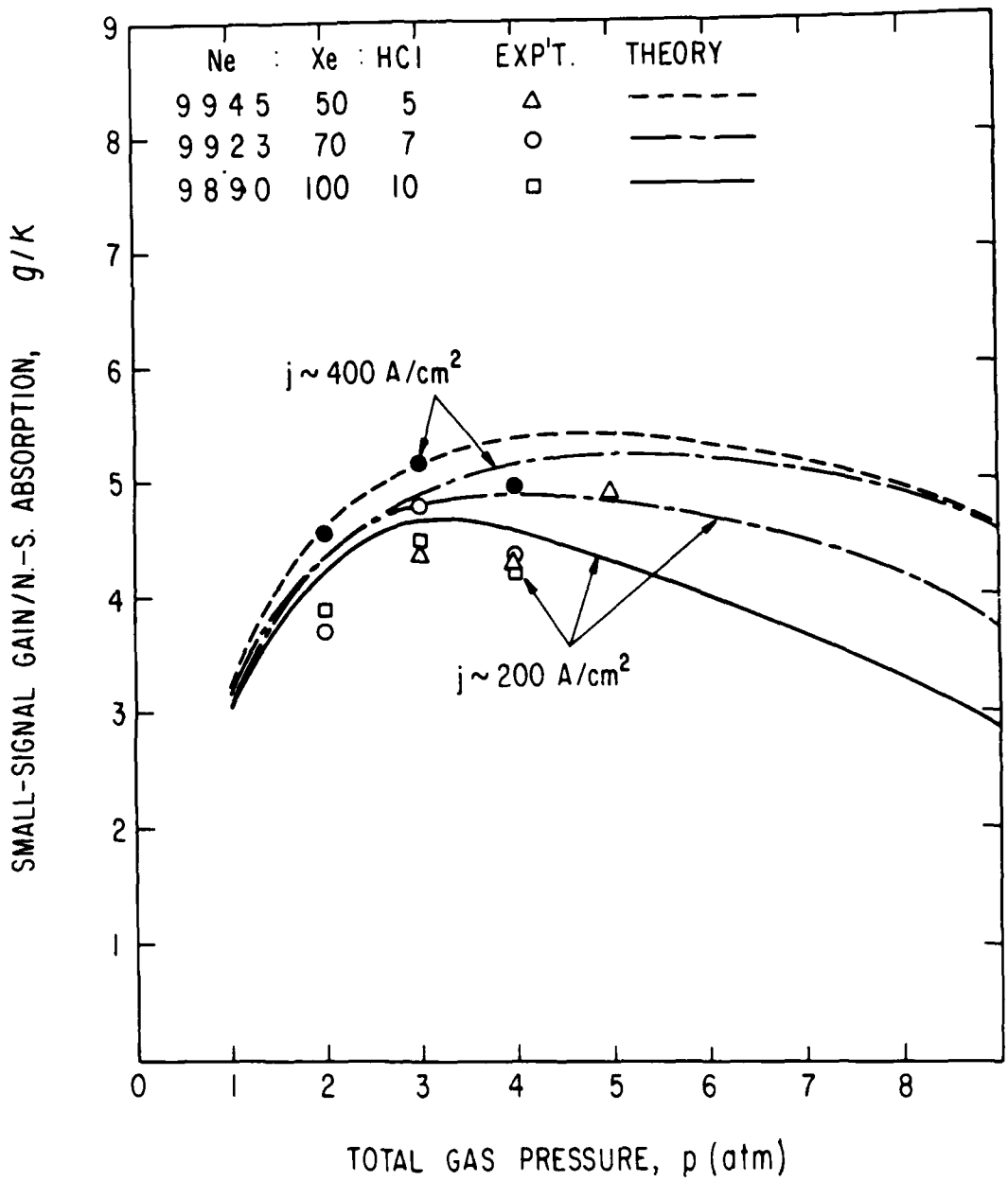

Fig. 11 (XIII) Ratio between the small-signal gain coefficient and the non-saturable absorption coefficient as deduced from the values of $g(\lambda_o)$ and $\kappa(\lambda_o)$ shown in Figs. 9 (XIII) and 10 (XIII).

but the current density was somewhat higher ($j \sim 0.6$ kA/cm^2). To obtain $g(\lambda_o)$ from a single measurement, Zheng et al[22] assumed that the value of $\kappa(\lambda_o)$ in the discharge-excited Ne/Xe/HCl plasma was known. Specifically, they used a constant value $\kappa(\lambda_o) = 0.025$ cm^{-1} taken from Refs. 24 and 25. In view of the variation of $\kappa(\lambda_o)$ with j observed in the present experiments (Fig. 10), the assumed value of 0.025 cm^{-1} appears to be too low for $j \sim 0.6$ kA/cm^2. This low value may have contributed to the factor of 2 discrepancy in $g(\lambda_o)$ determined from the two different experiments.

V. THEORETICAL INTERPRETATION

The variations of $g(\lambda_o)$ and $\kappa(\lambda_o)$ with current density, gas pressure, and mixture mol ratio (Figs. 9 and 10) can be interpreted in terms of the known kinetic processes in the discharge-excited XeCl laser.[24, 26, 27] However, in order to obtain good quantitative agreement between theory and experiment, we find it necessary to assume that the XeCl $B^2\Sigma_{1/2}$ excited state is one of the important contributors to the absorption processes at the laser-oscillation wavelengths, $\lambda_o = 307.94$ and 308.19 nm.

The theoretical curves plotted in Figs. 9, 10, and 11 for comparison with the experimental values of $g(\lambda_o)$ and $\kappa(\lambda_o)$, as well as the ratio $g(\lambda_o)/\kappa(\lambda_o)$, at two different values of j and three different mixture mol ratios at $j \sim 200$ A/cm^2, are based on a simplified kinetics model and a definite assignment of the excited-state absorption cross section $\sigma^* = 3.6 \times 10^{-17}$ cm^2 for the process

$$h\nu_o + XeCl^* \longrightarrow XeCl^{**}, \qquad (25)$$

where $XeCl^*$ denotes a xenon chloride excimer at the $B\,^2\Sigma_{1/2}$ state, and $XeCl^{**}$ represents some unidentified auto-ionized or auto-dissociated state of XeCl which lies above the B state with a Franck-Condon energy gap which is in resonance with the laser photon $h\nu_o$. The simplified model[27] retains all of the essential excitation, excimer formation, and quenching processes considered in Ref. 26 but assumes a quasi-steady-state balance of the production and destruction rates for the relevant excited species. The effect of a finite vibrational relaxation rate is also taken into account in determining the fraction of B-state molecules at the $v' = 0$ level, which contributed to the two strongest $B \rightarrow X$ laser transitions. The rotational population is assumed to be in quasi-equilibrium at an effective translational-rotational temperature $T \approx 320\ ^oK$, which is estimated from the mean Joule heating rate and pulse duration of the discharge. All spectroscopic data for the XeCl B and X states, including the Franck-Condon factors for the various pairs of vibrational levels, are taken from Ref. 16. The mean energy and energy distribution function of the free electrons, which govern the electron-impact excitation and attachment rates, are taken or extrapolated from earlier computer code calculations.[26] For all of the chemical species which never reach a quasi-steady-state population during the pulse discharge (e.g., HCl, H, Cl, etc.), time-averaged values deduced from earlier calculations[26] are used. Even though such a simplified model cannot be used for calculation of the transient plasma properties during the early and late phases of the discharge,

it is found to yield approximate numerical results which compare quite well with those obtained from detailed computer code calculations during the peak gain period (Fig. 8) for which the experimental points in Figs. 9, 10 and 11 are plotted. This model is, therefore, appropriate and economical to use for interpretation of experimental data over a wide range of parameters.

In addition to the excited-state absorption process (25), the following four absorption processes, with cross sections taken from Refs. 28, 29, 24, and shown in parentheses in units of cm^2, are also included in the theoretical calculation of $\kappa(\lambda_o)$ using our simplified model:

$$h\nu_o + Xe^* \longrightarrow Xe^+ + e \qquad (6.3 \times 10^{-20}), \qquad (26)$$

$$h\nu_o + Xe_2^* \longrightarrow Xe_2^+ + e \qquad (1.4 \times 10^{-17}), \qquad (27)$$

$$h\nu_o + Xe_2^+ \longrightarrow Xe^+ + Xe \qquad (2.5 \times 10^{-17}), \qquad (28)$$

$$h\nu_o + Cl^- \longrightarrow Cl + e \qquad (2.1 \times 10^{-17}), \qquad (29)$$

where Xe^* and Xe_2^* represent, respectively, Xe atom and Xe dimer in meta-stable excited electronic states, and e is a free electron. The absorption processes (25) through (29) are of the non-saturable type since the absorbing species are all immediately ionized or dissociated. The cross section $\sigma^* = 3.6 \times 10^{-17}$ cm^2 which we assumed in our simplified model for process (25) in order to obtain good agreement between theory and experiment, though somewhat larger than the published cross sections for processes (27), (28), and (29), is still of a reasonble magnitude for absorption into

an auto-ionized or auto-dissociated state. It is interesting to note that the major absorbing species considered in our theoretical model, Xe^*, Xe_2^*, Xe_2^+, Cl^-, and $XeCl^*$, are all generated by electron-impact processes, or, at least, generated through processes which are rate-limited by electron-impact processes. Accordingly, the number densities of these species during the quasi-steady-state phase of the pulsed discharge can be expected to be roughly proportional to the current density j. Thus, the value of $\kappa(\lambda_o)$ also can be expected to be roughly proportional to j as we have observed experimentally.

VI. DISCUSSIONS

The proposed method has been found to work well in our preliminary experiments. Determinations of $\kappa(\lambda_o)$ and $g(\lambda_o)$ from Eqs. (19) and (20) are found to be unambiguous, as long as the inserted cavity-loss coefficient κ_i is suitably chosen with respect to the net gain coefficient $G(\lambda_o)$ of the excited medium being studied. The range of value of $G(\lambda_o)$ must be sufficiently high in relation to the total time period over which such net gain can be maintained so that the laser oscillator can reach the assumed quasi-steady-state within some small fraction of the available inversion period. To minimize experimental scatter in repeated pulse measurements, the product of net gain and excitation length, $G(\lambda_o)L_m$, must also be sufficiently large in relation to the pulse-to-pulse amplitude fluctuations of $G(\lambda_o)$ and of the probe-beam intensity. In our preliminary experiments, the substantial pulse-to-pulse amplitude fluctuations of $I_1(\lambda_o)$ and $P_L(\lambda_o)$ (Figs. 6

and 7) were primarily due to the considerable time jitter of the self-triggered rail gap switches (Figs. 2 and 3). Such time jitter tended to make good synchronization between the preionization pulse and the main discharge pulse difficult. The complete lack of provisions for removal of waste products and for acoustic damping in the small discharge chambers may also have contributed to the observed amplitude fluctuations. Suitable improvements in the switching circuits and in the discharge chamber design would undoubtedly increase the signal-to-noise ratio and hence extend the range of experimental parameters over which the values of $g(\lambda_o)$ and $\kappa(\lambda_o)$ can be measured.

The proposed method is ideally suited for the determination of $g(\lambda_o)$ and $\kappa(\lambda_o)$ in atomic systems with homogeneously broadened spectral lines. For molecular systems with collision-broadened rotational lines and wide-band distributions of gain and absorption, as in the case of rare gas halogen excimers, spectrally-resolved measurements of $g(\lambda_o)$ and $\kappa(\lambda_o)$ associated with the individual rotational lines or with some narrow portions of the vibrational-rotational structures of the gain profile would require introduction of suitable wavelength-selection elements (e.g., gratings, etalons, etc.) into the probe beam generator and the laser oscillator. In the interpretation of these experimental data, the finite rates of vibrational-rotational energy transfer during the narrow-band stimulated emission process might have to be considered in the saturation analysis. In a narrow linewidth injection-locked laser oscillator experiment, Bourne and Alcock[21] have recently observed that the entire output of a high-pressure, discharge-pumped XeCl laser can be extracted within a very narrow linewidth, $\Delta\lambda = 4 \times 10^{-5}$ nm,

of the injected signal, as long as the injected signal wavelength was not too far off either the (0,1) or the (0,2) spectral peak of the XeCl B → X spontaneous emission (Fig. 5, upper spectrum). The discharge volume was $30 \times 1 \times 2$ cm^3 and the transmission line electrical length was 47 nsec. Other discharge parameters ($Ne:Xe:HCl:H_2 = 3040:20:4:5$ at $p = 4$ atm, $j \sim 2$ kA/cm^2) were quite comparable to those used in the discharge-pumped XeCl laser experiments reported in Refs. 5, 22, 23, and in the present experiments. The experiments of Bourne and Alcock[21] thus showed that, at least for some molecular laser systems such as the XeCl excimer laser at high gas pressures and high current densities, the rates of vibrational-rotational energy transfer within the upper and lower electronic states during the narrow-band stimulated emission process are so fast that the molecular band systems associated with the strong laser transitions behave very much like 2-level atomic systems with homogeneously broadened lines of very large spectral widths [i.e., equivalent values of γ_{ul} in Eqs. (13) and (14) comparable to the frequency-bandwidths of the corresponding molecular emission bands in the absence of stimulated emission]. If so, the simple formulation based on the 2-level system (Sec. 2) may still be valid for the determination of $g(\lambda_o)$ and $K(\lambda_o)$ in narrow-band measurements. We consider this to be a conjecture, which needs to be tested in suitably designed experiments.

It should be noted that during our derivation of the approximate formula for explicit determination of $K(\lambda_o)$ from the experimental values of $G(\lambda_o)$ and Γ for any fixed set of excitation conditions [Eq. (19)], we have implicitly assumed that the value of $K(\lambda_o)$ in the excited medium remained the

same during the two separate measurements illustrated in Fig. 1. This assumption is valid only when $\kappa(\lambda_o)$ is independent of, or, at least, insensitive to the laser radiation intensity. For the XeCl B → X laser, our preliminary experiments indicated that the upper laser level $B\,^2\Sigma_{1/2}$ may also be one of the most important absorbers. If so, $\kappa(\lambda_o)$ cannot be insensitive to the radiation intensity. Measurements of $G(\lambda_o)$ and $P_L(\lambda_o)$ at several overlapping intensities of the probe beam and of the beam waves within the saturated laser oscillator, together with suitable modifications of the laser amplifier and oscillator equations, may allow us to determine the intensity-dependence of $\kappa(\lambda_o)$ and also answer the question of whether the B state is, indeed, an important absorber in the XeCl B → X laser.

References

1. M. Rokni, J. A. Mangano, J. H. Jacob, and J. C. Hsia, IEEE J. Quant. Elect. QE-14, 464 (1978).
2. L. F. Champagne, L. J. Palumbo, and T. G. Finn, Appl. Phys. Lett. 34, 315 (1979).
3. G. C. Tisone and J. M. Hoffman, IEEE J. Quant. Elect. QE-18, 1008 (1982).
4. C. A. Brau,"Rare Gas Halogen Excimers," in Excimer Lasers, ed. by C. K. Rhodes, Springer-Verlag, Berlin Heidelberg New York (1979), pp. 85-133.
5. Q. H. Lou, Q. S. He, and S. C. Lin, Appl. Phys. Lett. 41, 514 (1982).

References for Section XIII (Continued)

6. W. E. Lamb, Jr., Phys. Rev. 134, A1429 (1964).

7. A. Icsevgi and W. E. Lamb, Jr., Phys. Rev. 185, 517 (1969)

8. G. D. Boyd and H. Kogelnik, Bell Sys. Tech. J. 41, 1347 (1962).

9. H. Kogelnik and T. Li, Proc. IEEE 54, 1312 (1966).

10. A. Yariv, Quantum Electronics, 2nd. ed., Wiley, New York (1975), Chapters 7 and 9.

11. A. G. Fox and T. Li, Bell Sys. Tech. J. 40, 453 (1961).

12. W. W. Rigrod, J. Appl. Phys. 34, 2602 (1963); 36, 2487 (1965).

13. L. F. Champagne, J. G. Eden, N. W. Harris, N. Djeu, and S. K. Searles, Appl. Phys. Lett. 30, 160 (1977).

14. L. F. Champagne, Appl. Phys. Lett. 33, 523 (1978).

15. J. Tellinghuisen, J. M. Hoffman, G. C. Tisone, and A. K. Hays, J. Chem. Phys. 64, 2484 (1976).

16. A. Sur, A. K. Hui, and J. Tellinghuisen, J. Molec. Spectrosc. 74, 465 (1979).

17. J. I. Levatter and Z. G. Li, Rev. Sci. Instrum. 52, 1651 (1981).

18. CVI Laser Corporation, technical data sheet.

19. CRC Handbook of Chemistry and Physics, CRC Press, Boca Raton, 63rd. ed. (1982-83), p. E-379.

20. Q. H. Lou, Q. S. He, and S. C. Lin, "Reversal of Spectral Narrowing of the XeCl B → X Spontaneous Emission Observed at High Gas Pressures," Paper J.6 presented at the International Conference

on Lasers '82, New Orleans, December 13 - 17, 1982.

21. O. L. Bourne and A. J. Alcock, Appl. Phys. Lett. 42, 777 (1983).

22. Zheng Chengen, Huo Yunsheng, and Wei Yunrong, Laser Journal (China) 10, 201 (1983).

23. S. C. Lin, Z. X. Bao, G. Y. Gong, Y. S. Huo, J. P. Shu, S. Q. Tang, Y. R. Wei, and C. E. Zheng, Appl. Phys. Lett. 38, 328 (1981).

24. L. A. Levin, S. E. Moody, E. L. Klosterman, R. E. Center, and J. J. Ewing, IEEE J. Quant. Elect. QE-17, 2282 (1981).

25. G. C. Tisone and J. M. Hoffman, Appl. Phys. Lett. 39, 145 (1981).

26. Y. S. Wang, Ph.D. Dissertation, University of California, San Diego (1982).

27. S. B. Zhu, Ph.D. Dissertation, University of California, San Diego (in progress).

28. K. J. McCann and M. R. Flannery, Appl. Phys. Lett. 31, 599 (1977).

29. D. C. Lorents, D. J. Ekstrom, and D. Huestis, Stanford Research Institute, Report MP 73-2 (1973).

XIV. REVERSAL OF SPECTRAL NARROWING OF XENON CHLORIDE $B\,^2\Sigma \rightarrow X\,^2\Sigma$ EMISSION OBSERVED AT HIGH GAS PRESSURES [++]

(S. C. Lin, Q. H. Lou, and Q. S. He, preliminary results presented at the International Conference on Lasers '82, New Orleans, U.S.A., December 13th to 17th, 1982; final paper in preparation for publication in the Journal of Quantitative Spectroscopy and Radiative Transfer)

Summary

For the rare gas halogen excimers, it is well known that the spectral width of the $B\,^2\Sigma \rightarrow X\,^2\Sigma$ spontaneous emission generally decreases with increasing gas pressure due to more rapid vibrational relaxation within the $B\,^2\Sigma$ excited electronic state. In some recent experiments, we have observed a re-broadening of the emission spectrum at gas pressures higher than a certain value p_r which is of the order of 5 atm, depending on the gas composition. Alternative interpretations of this re-broadening phenomenon are given and discussed.

[++] Work supported, in part, by the Defense Advanced Research Projects Agency under Contract N00014-76-C-0116 monitored by the Office of Naval Research, and by the National Science Foundation under Grant CPE82-19521.

1. INTRODUCTION

The emission spectra of several diatomic rare gas halogen excimers, especially XeF , XeCl , XeBr , XeI , and KrF , have been studied quite extensively in recent years.[1 - 8] These studies followed immediately the exploratory works of Golde and Thrush[9] and of Velazco and Setser[10] in 1974 and 1975, which subsequently stimulated a very rapid development of this important class of short-wavelength lasers.[11 - 16] The spectra were generated in flowing-afterglows at gas pressures ranging from 1 to several tens of torr, and in electron-beam-excited gas mixtures over the pressure range $0.3 < p < 3$ atm. The spontaneous emission spectrum from each excimer generally consists of several band systems. The strongest system is in the ultraviolet and has been assigned to the electronic transition $B\,^2\Sigma \rightarrow X\,^2\Sigma$. This band system also showed the strongest laser actions.[11 - 14] It is, therefore, most commonly used in the high power laser generation experiments in the ultraviolet.[17 - 24]

In one of the early papers, Brau and Ewing[2] had discussed at considerable length the difference in spectral widths of the $B\,^2\Sigma \rightarrow X\,^2\Sigma$ bands of XeCl and XeBr observed at high and low gas pressures. The low pressure spectra obtained from the flowing-afterglow experiments[10] were generally found to be much broader and also more diffuse than the high pressure spectra obtained from the e-beam excitation experiments.[2] Broadening of the low pressure spectra occurred mostly on the short wavelength side, usually in the form of an undulating but gradually decreasing intensity distribution which extends further into the ultraviolet with decreasing gas pressure. This has

been interpreted by Brau and Ewing [2] as a vibrational relaxation phenomenon associated with the excimer formation and radiation processes. That is, the $B\,^2\Sigma$ excimers were all formed by slow atomic (or ionic) collisions at large internuclear distances far removed from their respective potential energy minima.[16] Due to their strong ionic bonds and deep, tight potential wells, these newly formed excimers were left with large amounts of initial vibrational and rotational excitation. At the low gas pressures used in the flowing-afterglow experiments, vibrational relaxation was ineffective since the newly formed excimers could make very few, if any, subsequent collisions within the $\sim 10^{-8}$ sec radiative life time of the $B\,^2\Sigma$ state. Spontaneous emissions originating from the relatively populous excited vibrational levels $v' \geq 1$ would then account for the observed spread of the spectrum on the short-wavelength side. At the high gas pressures used in the e-beam-excitation experiments, vibrational relaxation was more rapid. The reduced radiation intensity from the $v' \geq 1$ levels thus caused the emission spectrum to appear narrower. This interpretation was found to be consistent with all subsequent experiments in which the method of excitation was fixed but the gas pressure was varied. Within each method of excitation, the spectral width $\Delta\lambda$ of the $B\,^2\Sigma \rightarrow X\,^2\Sigma$ spontaneous emission was always found to decrease with increasing gas pressure up to the highest pressures employed.[5, 14, 16, 25]

In this paper, we present some new experimental results from our recent measurement of $\Delta\lambda$ for the XeCl $B\,^2\Sigma \rightarrow X\,^2\Sigma$ spontaneous emission over the pressure range $0.6 < p < 15$ atm. The radiation source is a small (~ 1 cm^3), homogeneous volume, pulsed avalanche/self-sustained discharge

in dilute Ne/Xe/HCl and He/Xe/HCl mixtures at discharge current density $0.25 < j < 2\ kA/cm^2$. For convenient comparison with earlier works,[2] the spectral width $\Delta\lambda$ is defined here as the full-width at the half-maximum intensity point (FWHM) of the spontaneous emission spectrum plotted in the wavelength scale calibrated in air under typical laboratory conditions. As one would expect, the spectral width generally varies with the current density and mixture composition as well as with the total gas pressure. Because of the relatively high gas pressures employed, the numerical value of $\Delta\lambda$ observed in the present experiments is in the range of 1.1 to 1.7 nm, which is consistently narrower than the value of 2.3 nm observed in Ref. 2 at $p \approx 0.34$ atm in an e-beam excited $Ar:Xe:Cl_2 = 8992:1000:8$ mixture. The most significant result from the present experiments, however, is that the previously observed trend of decreasing spectral width with increasing gas pressure for a given gas mixture at a fixed excitation current density seems to continue only up to a certain pressure p_r. At pressures higher than p_r, the trend reverses and the spectral width becomes an increasing function of the gas pressure. The reversal pressure p_r, which can be defined as the gas pressure at which $\Delta\lambda$ reaches a minimum value, is found to be relatively insensitive to the current density j, but quite sensitive to the mixture composition. For example, when neon is used as the diluent gas in a mixture of initial mol ratio $Ne:Xe:HCl = 989:10:1$, the observed value of p_r is approximately 7 atm. When helium is used in place of neon as the diluent gas at the same mol ratio, the reversal pressure is reduced to $p_r \approx 4$ atm.

2. EXPERIMENTAL ARRANGEMENT

The experimental arrangement for generating the emission spectrum is illustrated in Fig. 1. The excimer molecules are continuously formed and destroyed during a homogeneous volume, pulsed avalanche/self-sustained discharge of approximately 200 nsec duration. The discharge is produced inside an x-ray preionized high pressure chamber of about 8 cm inside diameter and 7 cm maximum interior height. As described in Ref. 26, the discharge is driven by a transmission-line-type pulse forming network (not shown in diagram) of easily adjustable output impedance. The aluminum anode and cathode are of relatively large outer diameter ($\sim$ 5 cm) but the geometry and cross-sectional area of the discharge are precisely controlled within the central uniform-field region by the aperture opening of the x-ray preionization source. In the present experiments, the x-ray aperture is a round opening of 1.2 cm diameter and the separation distance d of the two opposing flat electrode surfaces is kept constant at 0.5 cm. Thus, the cross-sectional area of the discharge column is about 1 cm^2 and the total discharge volume is fixed at $\sim$ 0.5 cm^3.

The temporal variation of the total $B\,^2\Sigma \rightarrow X\,^2\Sigma$ spontaneous emission (fluorescence) intensity during the pulsed discharge is monitored through one of the two uv windows on the discharge chamber, using an ITT biplanar photodiode together with a 12 nm FWHM band-pass filter of 17% maximum transmittance at λ = 306 nm (Oriel No. 5703). For observation of the spectral distribution and for measurement of the spectral width of the XeCl $B\,^2\Sigma \rightarrow X\,^2\Sigma$ fluorescence, only time-integrated spectral are used in the present

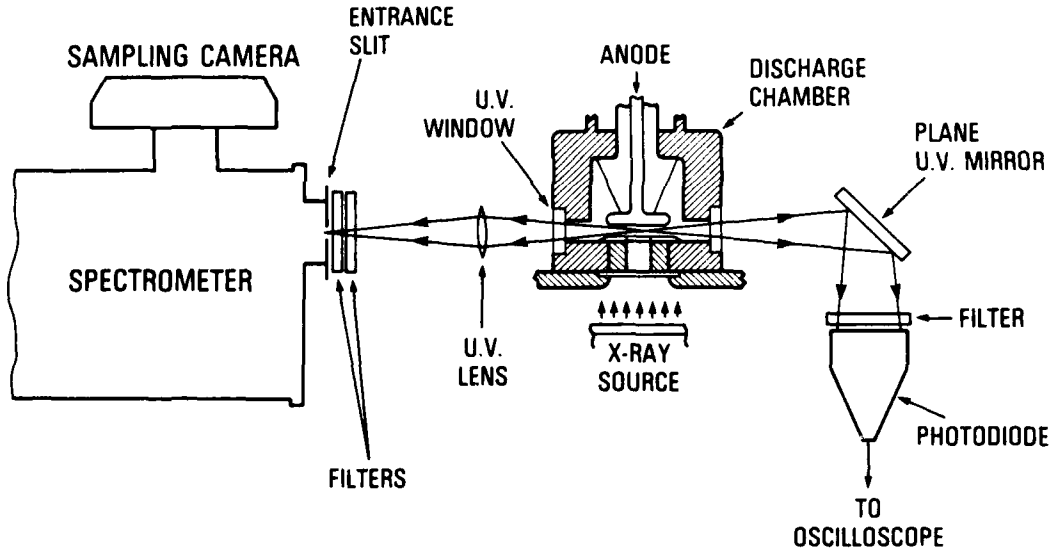

Fig. 1 (XIV) Experimental arrangement for taking time-integrated spectra of the XeCl B → X spontaneous emission from the small-volume, pulsed avalanche/self-sustained discharge, and for monitoring the temporal variations of the total emission intensity during the pulsed discharge.

study. As illustrated in Fig. 1, the time-integrated spectra are obtained by imaging the central portion of the 0.5 cm x 1.2 cm diameter discharge column onto the opened entrance slit of a spectrometer at approximately 1:1 magnification using a single-element fused silica lens of 2.5 cm diameter and 10 cm focal length. The spectrometer is actually a Spex Model 1401 3/4-meter Czerny-Turner double-grating monochromator/spectrometer with 102 x 102 mm gratings of 1200 grooves/mm blazed at λ = 500 nm and f/6.8 beam-forming mirrors. Since this instrument has a short-wavelength cut-off near the spectral peak of the XeCl $B\,^2\Sigma \rightarrow X\,^2\Sigma$ emission, only the second-order spectrum in the vicinity of $\lambda \sim 616$ nm is utilized for measurement of the spectral width $\Delta\lambda$. For improvement of the signal-to-noise ratio in this second-order spectrum, a uv band-pass filter with transmittance greater than 80% within the pass-band $300 < \lambda < 400$ nm and negligible (< 1%) transmittance for $\lambda > 500$ nm (Melles Griot filter No. 03FCG009) is inserted near the entrance slit of the spectrometer. To prevent over-exposure, neutral-density uv filters are also added occasionally.

The time-integrated spectra are recorded on Polaroid Type 665 films using the sampling camera provided by the Spex Model 1401 spectrometer. The camera actually samples only the output beam from the first diffraction grating so that the full noise rejection potential of this double-grating instrument is not being utilized. This, however, is unimportant since scattered light within the spectrometer has not been a significant source of error in our present study of the spectral width at the half-maximum-intensity point.

The Ne/Xe/HCl and He/Xe/HCl mixtures used in the discharge are prepared in a gas mixing system constructed of Monel and stainless steel. Chemically pure (CP grade) gases, typically of 99.9% purity rating, from commercial suppliers (Matheson, Airco, and MG Scientific Co.) are used without further purification. The gases are premixed in a stainless steel tank of 9.5 liter volume for 30 minutes or longer before being transferred into the discharge chamber. The mixing tank is equipped with a full-length, distributed-orifice mixing tube to ensure rapid homogeneous mixing at high gas pressures. The tank is also pre-evacuated to minimize initial contamination. For accurate determination of the pressure-dependence of $\Delta\lambda$, a single batch of gas mixture is normally employed for generating all the time-integrated spectra at the different gas pressures in sequential experiments.

3. SPONTANEOUS EMISSION PULSE SHAPE AND PULSE AMPLITUDE FLUCTUATION

Determination of the spectral width, $\Delta\lambda$, of the spontaneous emission intensity from the time-integrated spectra obtained in the manner just described requires specific knowledge of the photographic film sensitivity within the spectral region of interest. Accordingly, an <u>in situ</u> calibration of the Polaroid Type 665 film sensitivity in the vicinity of $\lambda \sim 616$ nm is carried out for each set of measurements. This is accomplished by a direct comparison of the developed film density of several photographic images of the XeCl $B\,^2\Sigma - X\,^2\Sigma$ second-order spectrum recorded on the same sheet of film under a fixed set of experimental conditions but at different cumulative exposures.

The cumulative exposure, in turn, is measured by the total number of consecutive discharge pulses used for forming the photographic image. This method of calibration does not require a precise control of the film development procedure, nor does it require a sheet-to-sheet reproducibility of the film sensitivity. The accuracy of this method, however, does depend on the pulse-to-pulse reproducibility of the spontaneous emission intensity from the discharge, especially when the number of consecutive pulses employed for forming each image is not very large.

In Fig. 2, we show some typical waveforms of the discharge voltage pulse and of the total XeCl $B\,^2\Sigma \rightarrow X\,^2\Sigma$ spontaneous emission intensity observed at different values of the initial gas pressure p and at two different levels of the self-sustained discharge current density j. The gas mixture is at a fixed initial mol ratio Ne : Xe : HCl = 989 : 10 : 1. The electrical length (2-way propagation time) of the transmission line for supplying the discharge current is fixed at 200 nsec and the initial voltage V_o on the transmission line at the time of avalanche initiation is also kept constant at approximately 26 kV. As previously noted in Ref. 26, the self-sustained discharge current observed in the small volume discharge is essentially a square pulse of $\sim$ 200 nsec duration and of amplitude $I \approx (V_o - V_{ss})/Z_o$, where Z_o is the output impedance of the transmission line, and V_{ss} is the self-sustaining voltage across the discharge plasma observed after the initial voltage collapse associated with the avalanche process but before the switching wave is reflected from the far end of the transmission line back to the plasma at $t \sim 200$ nsec.

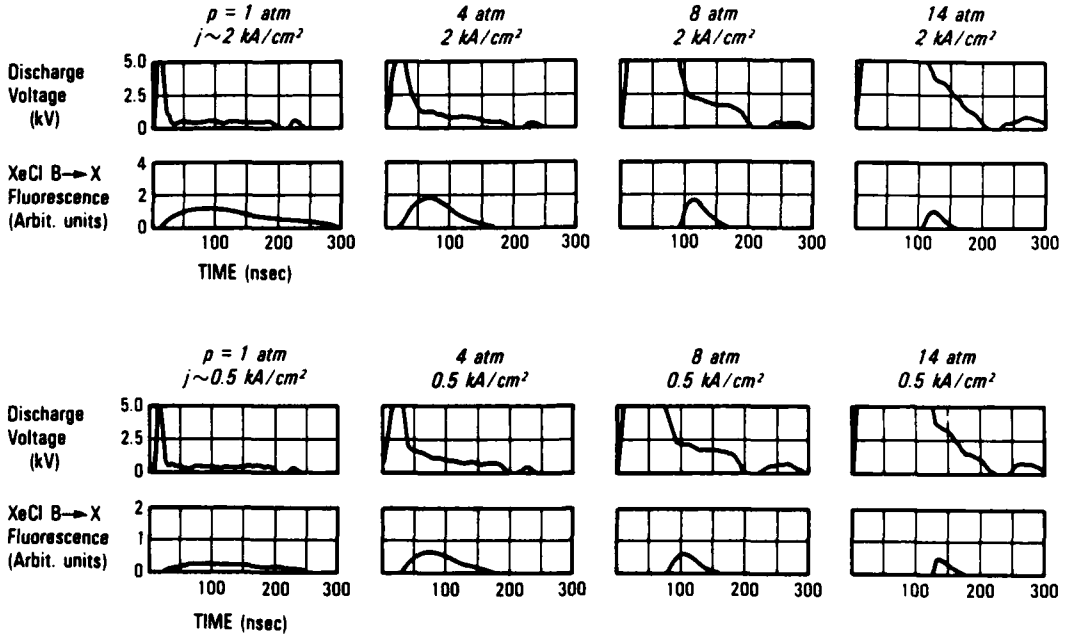

Fig. 2 (XIV) Typical waveforms of the discharge voltage and of the total XeCl B → X spontaneous emission intensity observed in the small cylindrical-volume (0.5 cm height, 1.2 cm diameter) discharge at a fixed transmission line pulse – charged voltage, $V_o \approx 26$ kV, and initial mixture mol ratio, Ne : Xe : HCl = 989 : 10 : 1. Note that at the higher gas pressures, the discharge voltage remains high and lies above the 2-cm vertical deflection limit of the monitoring oscilloscope (Tektronix 519) for a long period of time on account of the slow avalanche rate. The two different levels of the self-sustained discharge current density, $j \sim 2$ and 0.5 kA/cm^2, are obtained by changing the output impedance of the transmission line.

The voltage traces in Fig. 2 show that at the lower gas pressures, V_{ss} is approximately constant over the major fraction of the 200 nsec discharge period. As the gas pressure p increases, the time required for completion of the avalanche process becomes progressively longer so that the period of nearly constant V_{ss} becomes correspondingly shorter. The nearly constant V_{ss}, whenever observable, is roughly proportional to p but quite independent of j. These voltage characteristics are due to the facts that the net exponentiation rate of free electron number density, $d(\log n_e)/dt$, in a rare gas halogen mixture is a rapidly increasing function of the electric field strength to gas density ratio, E/n; and that the steady-state value $(E/n)_{ss}$ corresponding to $d(\log n_e)/dt = 0$ is approximately constant over a wide range of values of the electron mol fraction $[e] \equiv n_e/n$.[27, 28] In a homogeneously initiated electron avalanche sustained by a transmission-line-type pulse forming network,[29] there is no significant space charge field within the discharge gap d so that the local field strength is simply $E = V/d$. Upon initiation of the avalanche, the voltage V is a monotonically decreasing function of time so that the peak value of E/n, and consequently the maximum rate of electron exponentiation, are all limited by the initial voltage to gas pressure ratio, V_o/p. Thus, at a fixed V_o, the total time required for exponentiation of n_e from the initial preionization level n_{eo} to the quasi-steady-state level $(n_e)_{ss} \equiv (j/e v_e)_{ss}$, where e and v_e denote, respectively, the electronic charge and the electron drift velocity, can be expected to vary inversely with the initial gas pressure p. Since $(E/n)_{ss}$ is insensitive to n_e or j, the self-sustaining voltage, $V_{ss} \equiv (E/n)_{ss} n d$, can be expected to be proportional to the

initial pressure p and to remain approximately constant during the quasi-steady-state period of the pulsed discharge. The observed values of V_{ss} and of the avalanche completion time are generally in good quantitative agreement with recent theoretical model calculations.[28, 30]

From Fig. 2, it is seen that the waveform of the XeCl $B\,^2\Sigma \rightarrow X\,^2\Sigma$ spontaneous emission is roughly bell-shape, with an onset time at approximately the avalanche completion time and a peak value which varies with both the gas pressure p and current density j. As noted earlier in Ref. 26, the full-width at half-maximum intensity (FWHM) pulse duration of this emission at a given current density appears to decrease monotonically with increasing gas pressure. At a given gas pressure, the pulse duration is also found to decrease somewhat with increasing current density. These effects are most likely caused by more rapid quenching of the $B\,^2\Sigma$ excimers and more rapid depletion of the initial HCl mol fraction at higher values of p and j.

The pulse shape of the XeCl $B \rightarrow X$ emission is quite reproducible in repetitive discharges under a fixed set of experimental conditions. The pulse amplitude of this emission, however, is found to fluctuate randomly from pulse to pulse by an amount which varies with the gas pressure. Thus, at $p \leq 2$ atm, the maximum excursion of the pulse amplitude observed in 20 consecutive pulses is typically $\pm 6\%$ about the mean amplitude. At $p = 8$ atm, the maximum excursion is typically $\pm 11\%$. At $p = 14$ atm, the maximum excursion is increased to $\pm 24\%$. This amplitude fluctuation is primarily caused by the fluctuation in current density j in consecutive discharge pulses. The fluctuation in j, in turn, is due to variations in V_o and n_{eo} caused by

breakdown-voltage-fluctuation and time-jitter of the self-triggered rail gap switch used for transferring the pulse-charged transmission line voltage V_c to the discharge electrodes at the peak of the preionization pulse.[22, 26] The pulse-to-pulse fluctuations of the avalanche rate $d(\log n_e)/dt$ and of j can be expected to be more severe at the higher gas pressures on account of the more marginal initial E/n mentioned earlier.

4. DETERMINATION OF SPECTRAL WIDTH FROM THE TIME-INTEGRATED SPECTRUM

A typical sequence of the time-integrated spectrum of the XeCl $B\,^2\Sigma \rightarrow X\,^2\Sigma$ spontaneous emission recorded in the second-order by the sampling camera on the Spex 1401 double-grating spectrometer (Fig. 1) using Polaroid Type 665 film is reproduced in Fig. 3. For wavelength calibration, the neon line spectrum in the vicinity of $\lambda \sim 616$ nm recorded in the first-order by the same camera is also shown at the top and bottom. The small neon lamp (Oriel Model C-13-02) is placed in front of the 10 μm entrance slit of the spectrometer and aligned with the optical axis of the discharge chamber to ensure calibration accuracy. The gas mixture is at a fixed mol ratio Ne : Xe : HCl = 989 : 10 : 1 and the gas pressure is set sequentially at $p = 2$, 4, and 8 atm as indicated. The transmission line output impedance Z_o is fixed at 12.5 Ω and the avalanche-initiation voltage is, again, set at $V_o \approx 26$ kV. Using the self-sustained voltage V_{ss} indicated by the voltage traces in Fig. 2, we can readily deduce the self-sustained discharge current from the simple formula $I \approx (V_o - V_{ss})/Z_o$. The result is $I \approx 2.1$ kA at $p = 1$ atm and

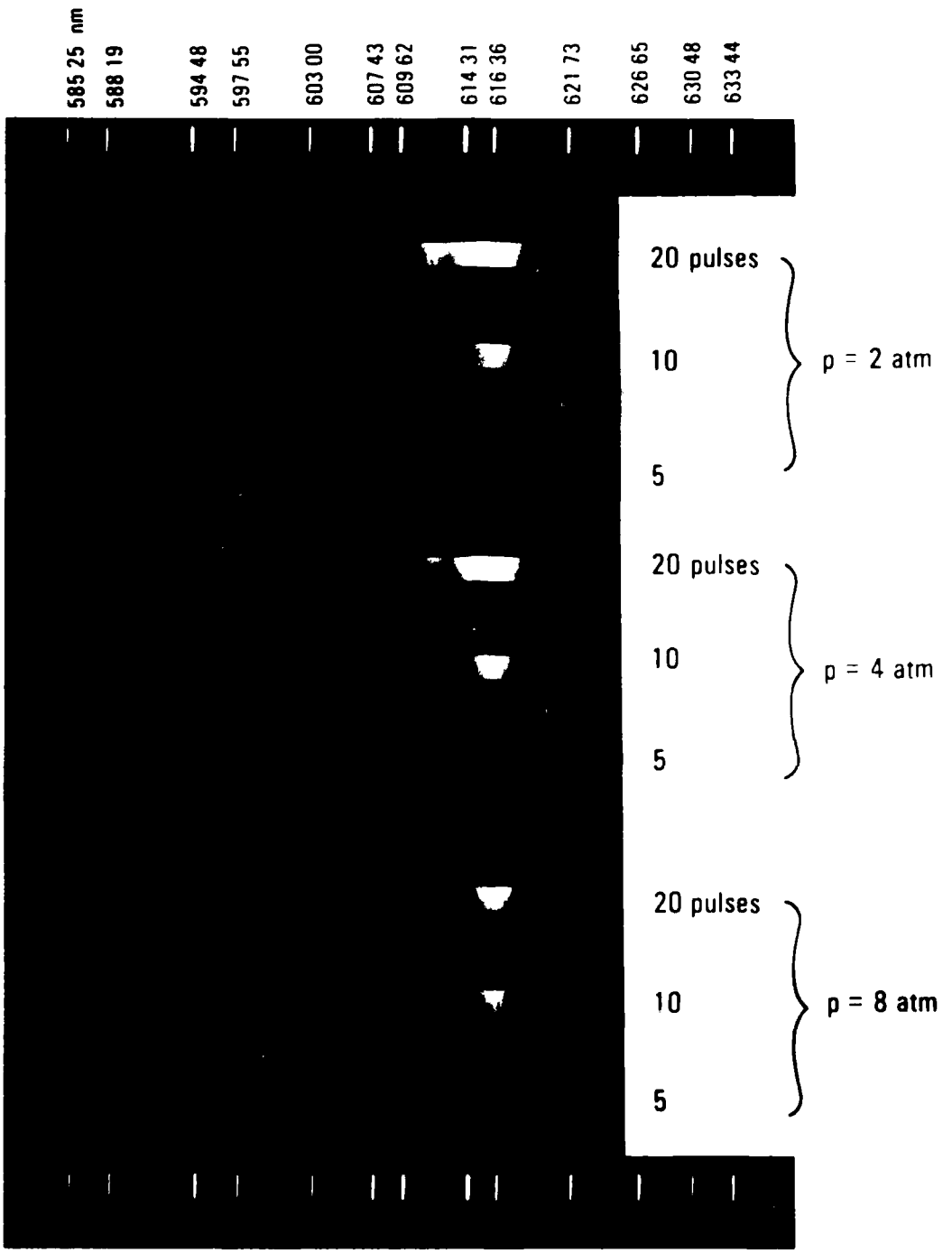

Fig. 3 (XIV) Samples of the time-integrated spectrum of the XeCl B → X spontaneous emission taken in the second-order at different gas pressures and with different cumulative exposures. Wavelength calibration is provided by the neon line-spectrum taken in the first-order.

$I \approx 1.9$ kA at $p = 8$ atm. Thus, the self-sustained current density within the 1.2-cm-diameter discharge column can be considered as essentially constant at $j \sim 2$ kA/cm^2 throughout this exposure sequence.

The three spectral images shown in Fig. 3 for each fixed value of p are obtained by time-integration of 20 , 10 , and 5 consecutive pulses , respectively, so that the total exposure is decreased by a factor of 2 in successive steps. The spectral resolution of the Spex 1401 spectrometer is about 0.004 nm at $\lambda = 308$ nm. In the image plane of the sampling camera, the dispersion is 2 mm/nm at $\lambda = 616$ nm. The Polaroid Type 665 film provides a positive-negative image pair for each exposure. The positive image is on opaque paper with a relatively poor resolution of 14 - 20 line pairs/mm. The negative image is on semi-transparent film with a 160 - 180 line pairs/mm spatial resolution, which is compatible with the dispersion and spectral resolution of the spectrometer using a 10 μm entrance-slit-width. Therefore, only the negative image is utilized for determination of the spectral width $\Delta\lambda$.

In Fig. 4, we show a typical strip-chart record of the photographic grain density of the developed negative image of the XeCl $B\,^2\Sigma \rightarrow X\,^2\Sigma$ emission spectrum over a relatively broad wavelength interval, $300 < \lambda < 311$ nm. The image is obtained from a 20-pulse exposure at $p = 2$ atm and $j \sim 2$ kA/cm^2, using an Ne : Xe : HCl = 989 : 10 : 1 mixture. The strip-chart record is obtained from a Jarrell-Ash Model 23-100 scanning microphotometer. The wavelength scale is deduced from the neon line spectrum taken on the same negative film where the XeCl second-order spectrum is recorded (Fig. 3). The gross features of this time-integrated spectrum, such as the

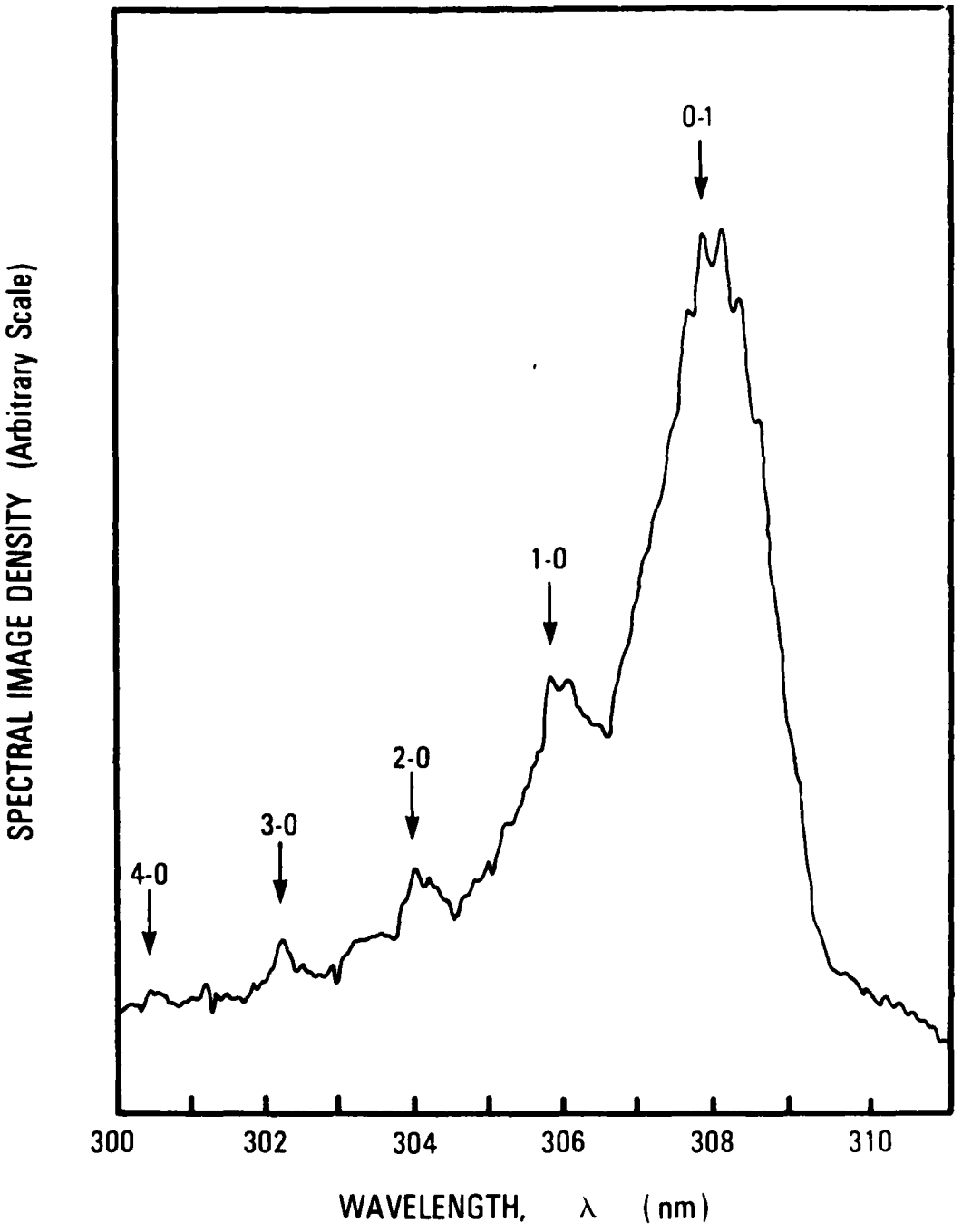

Fig. 4 (XIV) Relative spectral intensity distribution of the XeCl $B \rightarrow X$ spontaneous emission as measured by the image density of the time-integrated spectrum recorded in the second-order on Polaroid Type 665 negative film. The wavelength scale is deduced from the neon line-spectrum [Fig. 3 (XIV)].

main spectral peak at $\lambda \approx 308$ nm, the rapid fall-off of the spectral intensity on the long-wavelength side of the main peak, and the much slower fall-off of the spectral intensity on the short-wavelength side with undulating peaks of successively lower intensities which characterize the vibrational structure of the upper electronic state $B\,^2\Sigma$, are all quite similar to those observed by the earlier investigators at somewhat lower gas pressures.[2, 3, 8] The bandhead wavelengths corresponding to the various $v' \rightarrow v''$ vibrational transitions as assigned in Refs. 3 and 8 for the more abundant isotope component $Xe^{35}Cl$ are also marked by several vertical arrows for convenient identification of the successive secondary peaks in the emission spectrum.

Our method of <u>in situ</u> film sensitivity calibration for the sole purpose of spectral width determination can be explained by referring to the sample sets of densitometer traces illustrated in Fig. 5. These traces show the spectral image density distribution of the strongest emission bands around $\lambda \approx 308$ nm in somewhat more details than the one shown in Fig. 4. The bandhead locations for the various vibrational transitions $v' \rightarrow v''$ corresponding to the $v' = 0$ and 1 sequences as marked by vertical arrows above one set of traces are, again, taken from Refs. 3 and 8. Each set of traces is obtained by scanning three images developed on the same sheet of negative film in sequential exposures of the type shown in Fig. 3. The three images in each set correspond to the same discharge conditions ($j \sim 2$ kA/cm^2 in Ne : Xe : HCl = 989 : 10 : 1 mixture at $p = 1$, 4, 8, and 14 atm, respectively) but different cumulative exposures as indicated by the number of consecutive discharge pulses marked for each trace. All the traces shown here are generated at the same scanning speed

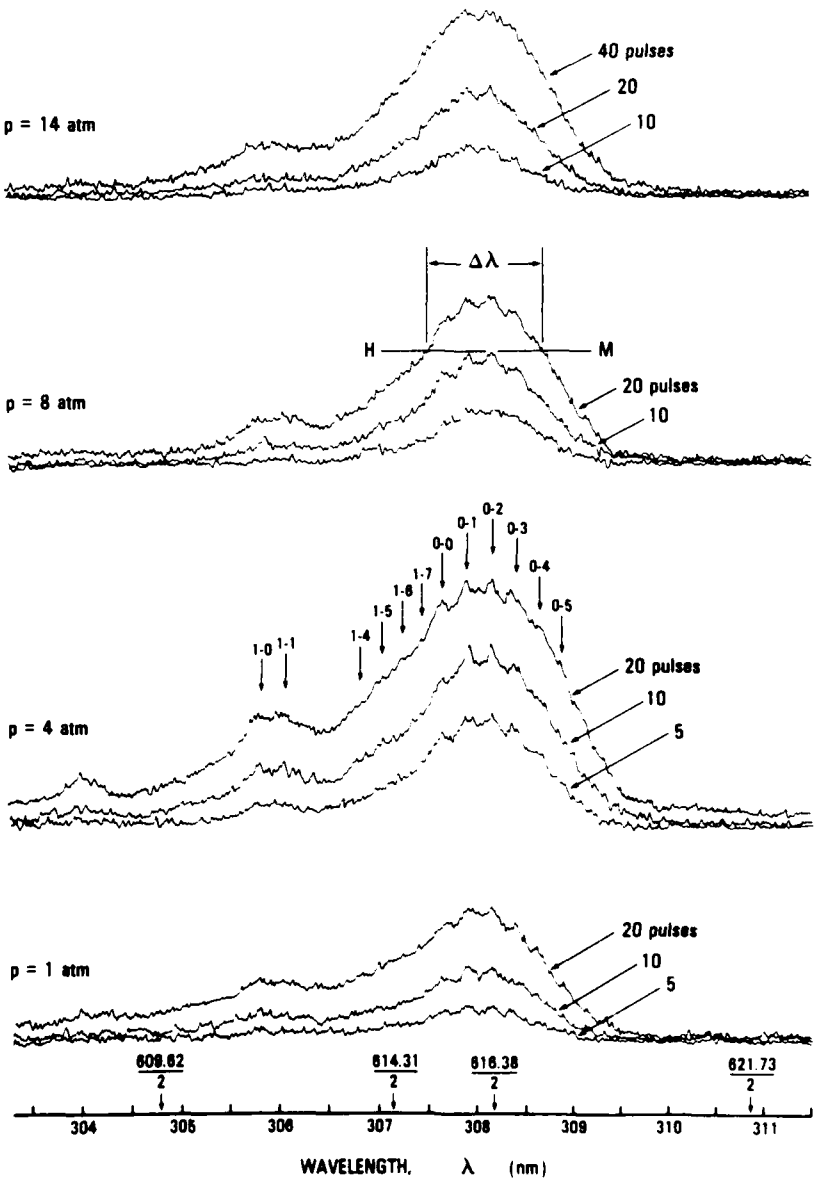

Fig. 5 (XIV) Samples of sequential densitometer traces of the time-integrated spectral image density used for determination of the spectral width, $\Delta\lambda$, of the XeCl B → X spontaneous emission. The three spectral images within each set correspond to exactly the same pulsed discharge conditions, but are different from each other by factors of 2 in cumulative exposures.

so that they share the same horizontal wavelength scale. The three densitometer traces within each image set are obtained at a fixed vertical sensitivity of the microphotometer servo loop and are also plotted from a common film background noise level corresponding to the unexposed (zero image density) regions, so that points of the same vertical height correspond to points of the same image density. Assuming that the spectral response of the photographic film is flat over the wavelength interval of interest, and that there exists a unique, but not necessarily linear, relationship between the local image density and the total local exposure within the same sheet of film, then the vertical heights of the densitometer traces so plotted can be used for mutual calibration of the total local exposure at different points of the three spectral images within the same set. Accordingly, the FWHM spectral width, $\Delta\lambda$, can be determined by locating the half-maximum exposure points on the spectral image through a proper height-comparison of any adjacent pair of densitometer traces within the same set which differ from each other only in cumulative exposure by exactly a factor of 2. This is illustrated in Fig. 5 where the horizontal line H - M is drawn through the peak of the middle trace corresponding to a 10-pulse cumulative exposure at $p = 8$ atm, and $\Delta\lambda$ is determined from the two intercept points of this line on the upper trace corresponding to a 20-pulse cumulative exposure within the same image set.

According to the technical data sheet supplied by the Polaroid Corporation (DS 13), the spectral sensitivity of the Type 665 negative film we use for taking the second-order spectrum at $\lambda \sim 616$ nm is not flat but degrades slightly toward the infrared at a rate of approximately 1% per nm. On the

AD-A141 203 STUDY OF AVALANCHE DISCHARGE LASERS(U) CALIFORNIA UNIV SAN DIEGO LA JOLLA INST FOR PURE AND APPLIED PHYSICAL SCIENCES S C LIN 30 SEP 83 N00014-76-C-0116 2/2

UNCLASSIFIED F/G 20/5 NL

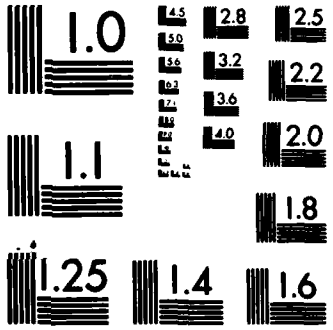

other hand, the spectral transmittance of the Melles Griot 03FCG009 filter we use for blocking the unwanted visible light at the entrance slit of the spectrometer (Fig. 1) is also not flat but degrades toward the vacuum uv at a rate of about 0.8% per nm at $\lambda \approx 308$ nm. Since the observed value of $\Delta\lambda$ in the present experiments is not much more than 1 nm (Section 5), the systematic error in $\Delta\lambda$ due to tilting of the spectrum by the combined non-uniform spectral properties of the film and of the filter is, therefore, smaller than 1%. In addition to this systematic error, however, there are two sources of statistical error which may be of greater significance. The first is the pulse-to-pulse amplitude fluctuation of the XeCl $B\,^2\Sigma \rightarrow X\,^2\Sigma$ spontaneous emission intensity (Section 3) which inevitably causes the cumulative exposures of the time-integrated spectral images corresponding to the upper and lower densitometer traces to deviate from the assumed exact 2 : 1 ratio. The second is an instrumentation noise due to the dithering motion of the strip chart recorder pen. This dithering motion, which manifested itself in the form of a random amplitude fluctuation of the densitometer traces (Fig. 5) with a mean period of $\sim$ 0.05 nm on the indicated wavelength scale, is found to be sensitive to the servo loop feedback setting on the microphotometer and is, therefore, somewhat controllable but cannot be completely eliminated. The magnitude of statistical error due to both sources can be reduced by increasing the number of consecutive discharge pulses used to form the spectral image sets and by taking averaged values of $\Delta\lambda$ determined from several image pairs for each set of discharge conditions.

5. EXPERIMENTAL RESULTS

The FWHM spectral width, $\Delta\lambda$, of the XeCl $B\,^2\Sigma \rightarrow X\,^2\Sigma$ spontaneous emission from the small volume discharge in dilute Ne/Xe/HCl and He/Xe/HCl mixtures has been measured over the pressure range $0.6 < p < 15$ atm using the method of image density comparison just described. In Fig. 6, we show a plot of $\Delta\lambda$ as a function of the initial gas pressure p observed at three different values of the self-sustained discharge current density j in a Ne:Xe:HCl = 989:10:1 mixture. Each plotted point represents the averaged value of $\Delta\lambda$ measured from four image pairs taken from five sequential spectral images of the type illustrated in Fig. 3. At the lower gas pressures, the five images are obtained from an exposure sequence of 5, 10, 20, 10, and 5 consecutive discharge pulses for each image, respectively, at a repetition rate of approximately 1 pulse/sec. At the higher gas pressures, the number of consecutive discharge pulses employed in the exposure sequence is increased to 10, 20, 40, 20 and 10. The vertical bars drawn about some of the plotted points indicate the maximum spread of the four measured values of $\Delta\lambda$, while the plotted points without vertical bars indicate that the four measured values of $\Delta\lambda$ are closely bunched. The three curves fitted through the three sets of experimental points corresponding to the three different approximate values of j clearly show that at a fixed current density, the spectral width $\Delta\lambda$ first decreases with increasing gas pressure, reaching a minimum value at $p \approx 7$ atm, and then increases again at the higher gas pressures. All three curves are similar in shape and are vertically separated from each other only by a few percent of the mean value, indicating that the dependence of $\Delta\lambda$

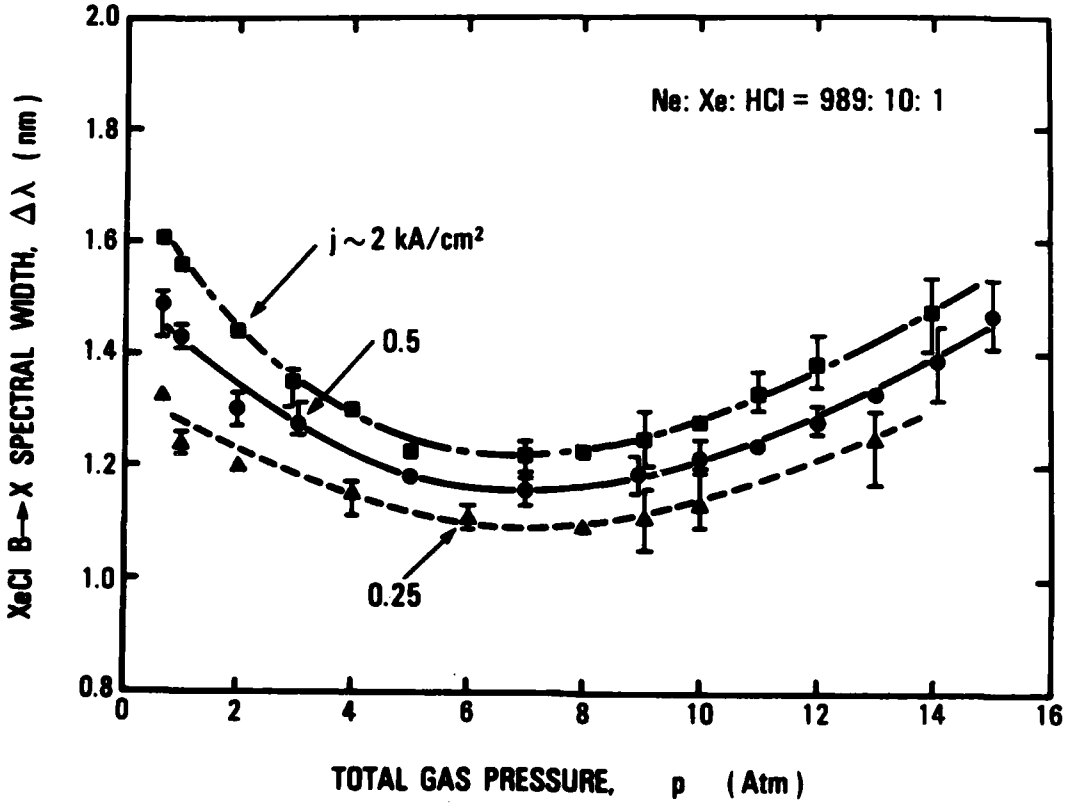

Fig. 6 (XIV) Full width at half-maximum intensity of the XeCl B → X spontaneous emission, $\Delta\lambda$, as a function of the total gas pressure p observed in the small-volume discharge at three different levels of the pulsed current density j. The gas mixture is of initial mol ratio Ne : Xe : HCl = 989 : 10 : 1. Each plotted point represents the averaged value of $\Delta\lambda$ measured from four pairs of sequential densitometer traces [Fig. 5 (XIV)]. The maximum spread of the measured values of $\Delta\lambda$, if greater than the height of the plotted point, is indicated by the associated vertical bar.

on j is relatively weak. In fact, the fitted curves show that the minimum spectral width, $(\Delta\lambda)_{min}$, at the reversal pressure $p_r \approx 7$ atm, varies only roughly between 1.1 and 1.2 nm over the current-density range $0.25 < j < 2$ kA/cm^2. At a fixed j, the amount of re-broadening of $\Delta\lambda$ at twice the reversal pressure, $p = 2p_r \approx 14$ atm, is approximately 20% of the corresponding value of $(\Delta\lambda)_{min}$. As indicated by the vertical bars, the maximum deviation of $\Delta\lambda$ from its local mean value is only about 5%. The observed reversal of the narrowing trend of the XeCl $B\,^2\Sigma \rightarrow X\,^2\Sigma$ emission spectrum at gas pressures greater than p_r is, therefore, very clear and unmistakable.

In Fig. 7, we show the effect of using helium in place of neon as the diluent gas on the spectral width. Here, the self-sustained discharge current density is fixed at $j \sim 0.5$ kA/cm^2. The initial mixture mol ratio is kept constant at He : Xe : HCl = Ne : Xe : HCl = 989 : 10 : 1. The fitted experimental curves show that, upon replacement of neon by helium, the reversal pressure p_r is down-shifted from 7 atm to about 4 atm and the corresponding value of $(\Delta\lambda)_{min}$ is increased slightly from 1.16 to about 1.22 nm. Above the respective values of p_r, the gas pressure at which a 20% re-broadening of $\Delta\lambda$ is observed is also down-shifted from $p \approx 14$ atm to $p \approx 9$ atm.

As mentioned earlier in Sec. 2, the temporal variation of the total (spectrally-integrated) XeCl $B\,^2\Sigma \rightarrow X\,^2\Sigma$ spontaneous emission intensity is monitored by an ITT biplanar photodiode concurrently with the photographic recording of the time-integrated spectrum (Fig. 1). In Fig. 8, we show the peak intensity of this total spontaneous emission corresponding to the various experimental conditions of Fig. 6 and 7, all plotted on the same relative scale.

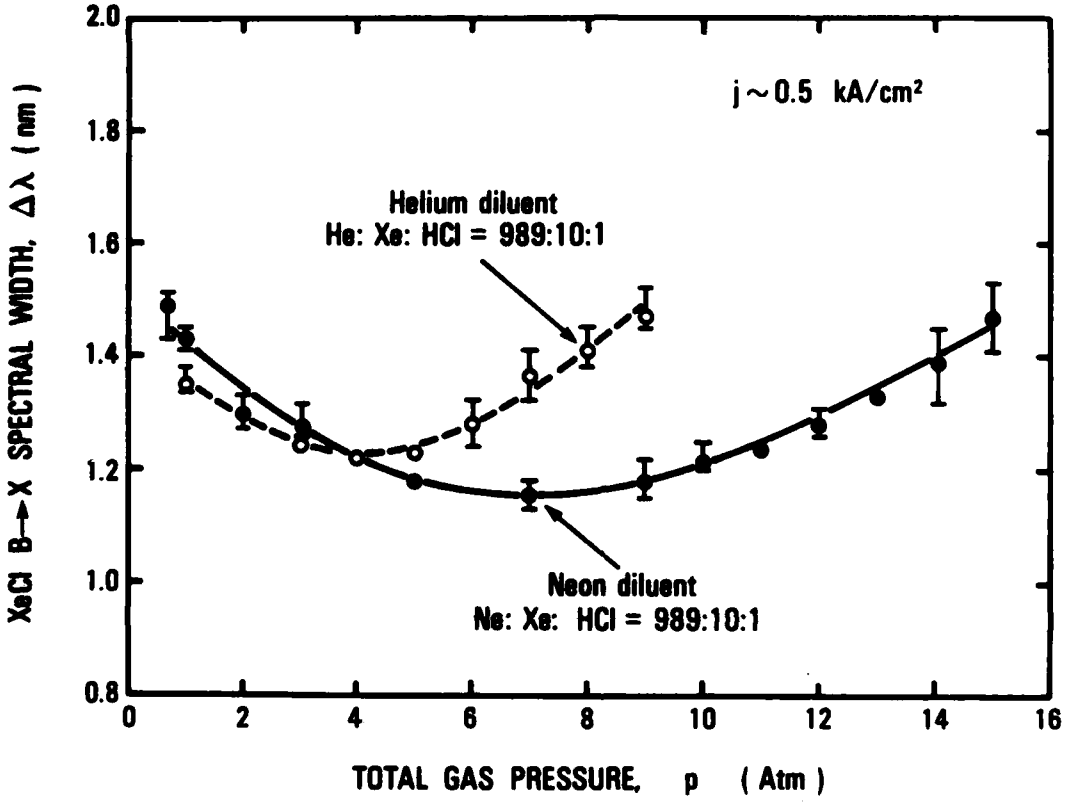

Fig. 7 (XIV) Experimental results showing the effect of changing the diluent gas from neon to helium on the measured value of $\Delta\lambda$. Both sets of experimental points are obtained at the same level of the pulsed current density, $j \sim 0.5$ kA/cm^2, and the same initial mixture mol ratio, He : Xe : HCl = Ne : Xe : HCl = 989 : 10 : 1. A definite shift of the reversal pressure p_r is quite evident from the two curves fitted through the mean values of the respective $\Delta\lambda$.

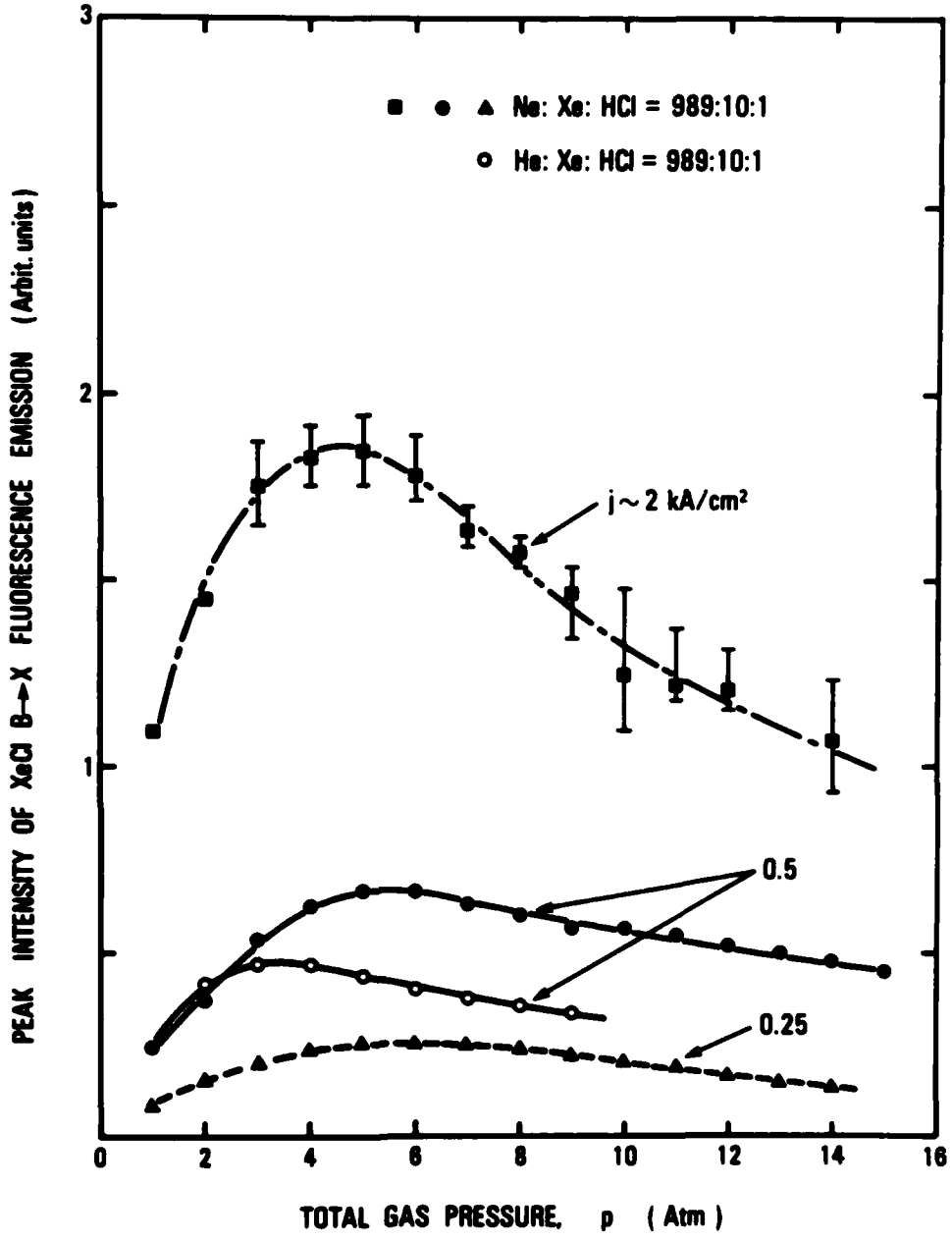

Fig. 8 (XIV) Variation of the peak value of the total (spectrally-integrated) XeCl B → X spontaneous emission intensity with the gas pressure p, the current density j, and the choice of diluent gas observed in the small-volume, pulsed avalanche/self-sustained discharge using a Ne:Xe:HCl = He:Xe:HCl = 989:10:1 mixture.

The vertical position of each plotted point indicates the averaged pulse-height of the photodiode output, which is assumed to be directly proportional to the XeCl B → X fluorescence intensity (Fig. 2). The vertical bars drawn about some of the points represent typical fluctuations of the pulse-height observed in random sampling of 5 consecutive discharge pulses. These results show that, in contrast to the very weak current-density-dependence of $\Delta\lambda$ (Fig. 6), the spontaneous emission intensity does depend strongly on the current density as one would expect from a general consideration of the XeCl excimer formation kinetics.[28, 30] At a fixed current density and for a given gas mixture, there exists an optimum gas pressure for maximizing the XeCl $B\,^2\Sigma$ population density and the XeCl B → X spontaneous emission intensity. Such an optimum pressure is determined by a competition between the excimer formation rate and the collisional quenching rate. The curves fitted through the experimental points in Fig. 8 indicate that for $0.25 < j < 2$ kA/cm^2, the optimum gas pressure is in the range of 4 to 6 atm for the Ne : Xe : HCl = 989 : 10 : 1 mixture and somewhat lower for the He : Xe : HCl = 989 : 10 : 1 mixture. Thus, there appears to be some correlation between this optimum gas pressure with the reversal pressure p_r defined earlier (Figs. 6 and 7), and with the gas pressure at which the XeCl B → X laser emission from the small volume discharge was also observed to be the strongest.[26]

6. DISCUSSIONS

According to Tellinghuisen et al.,[3, 8] the observed spectral intensity distribution of the XeCl B → X spontaneous emission in the ultraviolet is the

result of many overlapping vibrational/rotational bands from the various isotope components of XeCl. The bandhead locations assigned to some specific vibrational transitions, $v' \rightarrow v''$, for the more abundant component, $Xe^{35}Cl$, are as indicated by the vertical arrows in Fig. 5. The emission intensity from each band spreads only to the shorter-wavelength-side of the bandhead. Rotational analysis was incomplete since the rotational structure could only be partially resolved in some bands.[8] At high-v'', the rotational structure tends to break off into diffuse emission at fairly low N, as the $X\,^2\Sigma$ level becomes rotationally unbound.

The emitting gas sample from the small-volume discharge is optically-thin,[31] so that the partial spectral intensities from all the bands are additive. The relative contributions from the various bands to the total spontaneous emission intensity are, therefore, weighted by the population of the $B(v')$ level and by the Franck-Condon density[8] for the corresponding $B(v') \rightarrow X(v'')$ transition. As indicated in Fig. 5, the primary contributions to the peak intensity of the XeCl $B \rightarrow X$ spontaneous emission are from the 0 - 1, 0 - 2, and 0 - 3 bands over the wavelength interval $307.9 \leq \lambda \leq 308.2$ nm. In the vicinity of the half-maximum-intensity points, $\lambda \approx 307.5$ and 308.7 nm, the primary contributions appear to come from several high-v'' bands in the $v' = 1$ and $v' = 0$ sequences, respectively, as well as from spreading of the 0 - 0, 0 - 1, and 0 - 2 band intensities into the shorter wavelengths. By using the method of <u>in situ</u> film sensitivity calibration described in Section 4, we can deduce that at $p = 1$ atm, the intensity ratio between the 1 - 1 band at $\lambda \approx 306$ nm and the 0 - 1 band at $\lambda \approx 308$ nm is approximately 1/2.

At the three higher gas pressures, p = 4 , 8 , and 14 atm, this intensity ratio is about a factor-of-2 lower and assumes a nearly constant value, $I_{11}/I_{01} \approx 1/4$.

The initial decrease of I_{11}/I_{01} when p is increased from 1 to 4 atm can be attributed to a decrease in population of the v' = 1 level relative to that of the v' = 0 level due to more rapid vibrational relaxation as noted by the earlier investigators (Section 1). A corresponding decrease in emission intensities from the high-v'' bands in the v' = 1 sequence may account for the observed narrowing of $\Delta\lambda$ with increasing gas pressure. At $p \geq 4$ atm, vibrational relaxation may be close to completion so that the population of the v' levels may approach the equilibrium distribution corresponding to the prevailing kinetic temperature. Vibrational relaxation then ceases to be a significant factor in governing $\Delta\lambda$. The experimentally observed intensity ratio, $I_{11}/I_{01} \approx 1/4$, is quite consistent with the theoretical quasi-equilibrium value, $(I_{11}/I_{01})_{eq.} \approx 0.20$, which can be calculated from the Franck-Condon density ratio published in Ref. 8, and a kinetic temperature T = 450 ^{o}K based on adiabatic joule-heating of the Ne:Xe:HCl = 989:10:1 mixture at p = 4 atm and $j \sim 2$ kA/cm^2 during the peak of the XeCl B → X fluorescence pulse (Fig. 2).

There are several possible interpretation of the observed re-broadening of $\Delta\lambda$ at $p > p_r$ (Figs. 6 and 7) which are consistent with a constant population ratio between the v' = 1 level and the v' = 0 level implied by the invariance of I_{11}/I_{01} . The simplest explanation is collision-broadening of the individual rotational lines, or of the entire rotational structure, of

all the strong emission bands which contribute to $\Delta\lambda$ (Fig. 5). Approximate calculations by Zhu[30] using the quasi-equilibrium model (with interpolated rotational constants from Ref. 8) indicate that if all the rotational lines were emitting independently and were collision-broadened to the same Lorentzian width, an optical cross-section of the order of 10^{-14} cm^2 could produce a re-broadening of $\Delta\lambda$ at $p > p_r$ comparable to what is experimentally observed. Reliable estimate of the collision-broadening effects on the XeCl $B \rightarrow X$ emission spectrum, however, is actually quite difficult in view of the uncertain rotational structure and the partially-bound-free nature of the $B(v') \rightarrow X(v'')$ transitions involving the high-v'' levels.

An alternative interpretation of the $\Delta\lambda$-re-broadening phenomenon is that the pressure-induced (or collision-induced) effects on the $v' \rightarrow v''$ emission intensities tend to favor the high-v'' bands within the $v' = 0$ and $v' = 1$ sequences. For example, it is well known that collisional quenching is a dominant factor in suppressing the spontaneous emission rates in most rare gas halogen excimers at high gas pressures.[32] Thus, if the partial quenching rate coefficients for the individual $v' \rightarrow v''$ emissions do depend on v' and v'' in a manner similar to the corresponding Franck-Condon factors,[8] the quenching collisions would suppress the low-v'' emissions in the vicinity of the spectral peak, $\lambda \approx 308$ nm, more severely than the high-v'' emissions in the vicinity of the half-maximum-intensity points, $\lambda \approx 307.5$ and $\lambda \approx 308.7$ nm. The net result is an apparent increase of $\Delta\lambda$ with increasing p after collisional quenching becomes a dominant factor in limiting the total spontaneous emission rate (Fig. 8).

References for Section XIV

1. J. J. Ewing and C. A. Brau, Phys. Rev. A12, 129 (1975).
2. C. A. Brau and J. J. Ewing, J. Chem. Phys. 63, 4640 (1975).
3. J. Tellinghuisen, J. M. Hoffman, G. C. Tisone, and A. K. Hays, J. Chem. Phys. 64, 2484 (1976).
4. J. Tellinghuisen, G. C. Tisone, J. M. Hoffman, and A. K. Hays, J. Chem. Phys. 64, 4796 (1976).
5. J. E. Velazco, J. H. Kolts, and D. W. Setser, J. Chem. Phys. 65, 3468 (1976).
6. J. Tellinghuisen, A. K. Hays, J. M. Hoffman, and G. C. Tisone, J. Chem. Phys. 65, 4473 (1976).
7. P. C. Tellinghuisen, J. Tellinghuisen, J. A. Coxon, J. E. Velazco, and D. W. Setser, J. Chem. Phys. 68, 5187 (1978).
8. A. Sur, A. K. Hui, and J. Tellinghuisen, J. Molec. Spectrosc. 74, 465 (1979).
9. M. F. Golde and B. A. Thrush, Chem. Phys. Lett. 29, 486 (1974).
10. J. E. Velazco and D. W. Setser, J. Chem. Phys. 62, 1990 (1975).
11. S. K. Searles and G. A. Hart, Appl. Phys. Lett. 27, 243 (1975).
12. J. J. Ewing and C. A. Brau, Appl. Phys. Lett. 27, 350 (1975).
13. E. R. Ault, R. S. Bradford, Jr., and M. L. Bhaumik, Appl. Phys. Lett. 27, 413 (1975).
14. C. A. Brau and J. J. Ewing, Appl. Phys. Lett. 27, 435 (1975).
15. J. A. Mangano and J. H. Jacob, Appl. Phys. Lett. 27, 495 (1975).

References for Section XIV (Continued)

16. C. A. Brau, "Rare Gas Halogen Excimers," in Excimer Lasers (Edited by C. K. Rhodes) pp. 85 - 133, Springer-Verlag, Berlin (1979).

17. M. L. Bhaumik, R. S. Bradford, Jr., and E. R. Ault, Appl. Phys. Lett. 28, 23 (1976).

18. B. Godard and M. Vannier, Opt. Commum. 18, 206 (1976).

19. R. Burnham and N. Djeu, Appl. Phys. Lett. 29, 707 (1976).

20. R. O. Hunter, C. Howton, and J. Oldenettel, "Large Scale Discharge Pumped Molecular Halogen Lasers," AIAA 15th Aerospace Sciences Meeting, Los Angeles, California, January 24 - 26, 1977, Paper 77-26 (1977).

21. W. J. Sarjeant, A. J. Alcock, and K. E. Leopold, IEEE J. Quant. Elect. QE-14, 177 (1978).

22. S. C. Lin and J. I. Levatter, Appl. Phys. Lett. 34, 505 (1979).

23. S. C. Lin, Z. X. Bao, G. Y. Gong, Y. S. Huo, J. P. Shu, S. Q. Tang, Y. R. Wei, and C. E. Zheng, Appl. Phys. Lett. 38, 328 (1981).

24. J. I. Levatter, K. L. Robertson, and S. C. Lin, Appl. Phys. Lett. 39, 297 (1981).

25. J. H. Kolts, J. E. Velazco, and D. W. Setser, J. Chem. Phys. 71, 1247 (1979).

26. Q. H. Lou, Q. S. He, and S. C. Lin, Appl. Phys. Lett. 41, 514 (1982).

References for Section XIV (Continued)

27. H. H. Luo, Ph. D. Dissertation, University of California, San Diego (1978).

28. Y. S. Wang, Ph. D. Dissertation, University of California, San Diego (1982).

29. J. I. Levatter and S. C. Lin, J. Appl. Phys. 51, 210 (1980).

30. S. B. Zhu, Ph. D. Dissertation, University of California, San Diego (1984).

31. S. C. Lin, S. B. Zhu, Q. H. Lou, and Q. S. He, J. Quant. Spectrosc. and Radiative Transfer, 31, (1984).

32. M. Rokni, J. A. Mangano, J. H. Jacob, and J. C. Hsia, IEEE J. Quant. Elect. QE-14, 464 (1978).

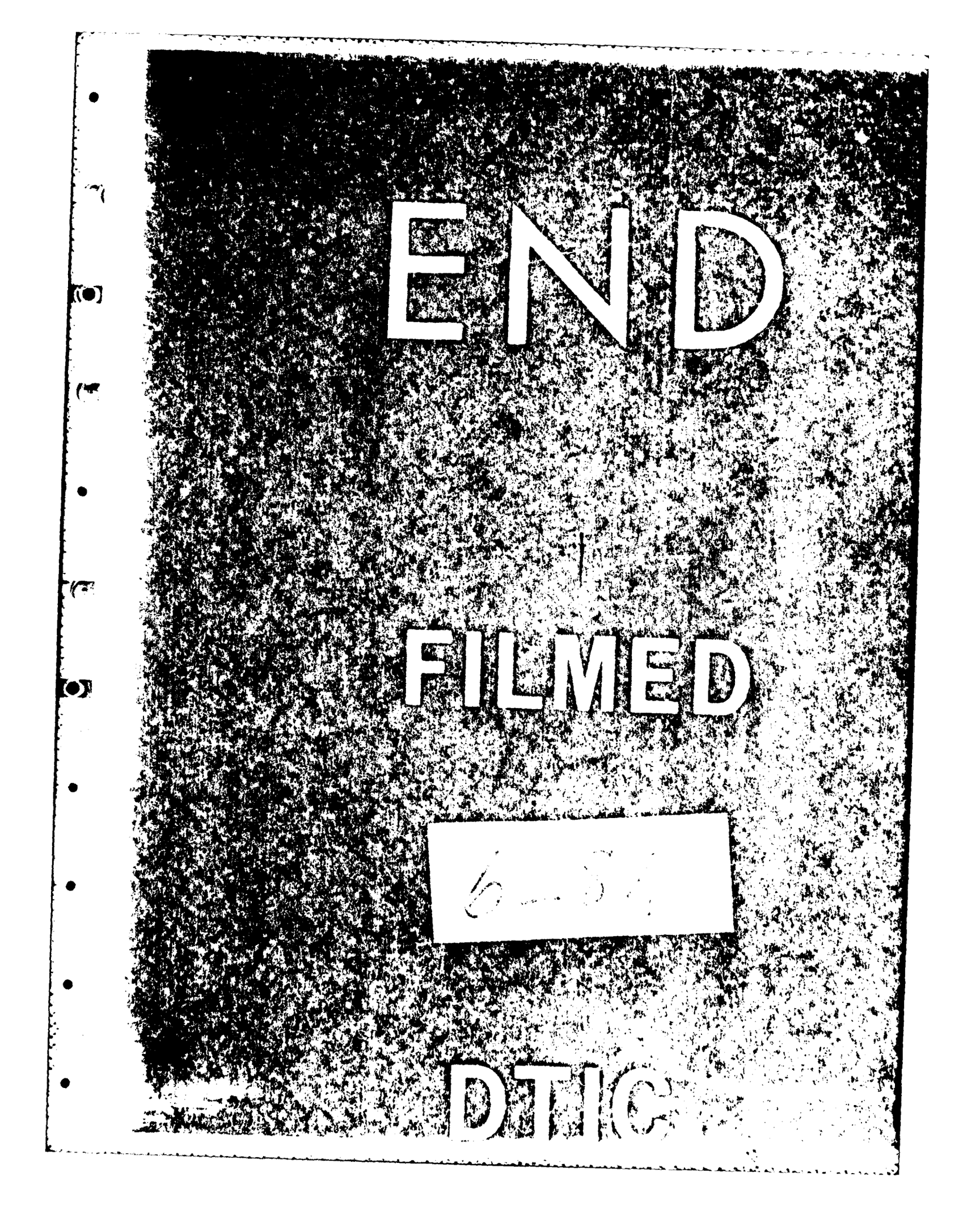
END
FILMED
DTIC